1-1-2016

Synthesis and Electrochemical Performance of Hydrothermally Synthesized Co3O4 Nanostructured Particles

Hitesh Adhikari

SYNTHESIS AND ELECTROCHEMICAL PERFORMANCE OF HYDROTHERMALLY SYNTHESIZED Co_3O_4 NANOSTRUCTURED PARTICLES

by

Hitesh Adhikari

A Thesis

Submitted in Partial Fulfillment of the

Requirements for the Degree of

Master of Science

Major: Physics

The University of Memphis

August 2016

DEDICATED TO MY PARENTS

ACKNOWLEGEMENTS

I would like to express my deepest gratitude to my adviser Professor Sanjay R. Mishra for his guidance and continual support during the course of my research. I would also like to express my appreciation to my committee members, Professor M. S. Jahan and Professor J. Cui for their time and effort to make my research successful. My sincere gratefulness goes to the Department of Physics and Materials Science for providing me an opportunity to pursue Master's degree with full financial support. I am thankful to Dr. Ram Gupta from Pittsburg State University, Pittsburg, Kansas, for his assistance on capacitive measurements of samples. I would also like to thank Dr. Jahangir Alam, who has provided technical help in my project. I express my appreciation to all the professors of the department of Physics and Materials science for their valuable guidance towards my academia.

I would like to thank my friends and all the supportive ones who directly or indirectly helped me to make my thesis successful. I am grateful to my family whose love and support made me successful to accomplish whatever I have so far. Finally, but not the least, my wife Arpana Poudyal for supporting me in every step of my career.

ABSTRACT

Adhikari, Hitesh. M.S. The University of Memphis. August 2016. Synthesis and Electrochemical Performance of Hydrothermally Synthesized Co_3O_4 Nanostructured Particles Major Professor: Sanjay R. Mishra, Ph. D.

Spinel Co_3O_4 exhibit remarkable photo- and electro-chemical properties. Combined with its cost effectiveness and wide abundance, Co_3O_4 has emerged as a promising candidate for pseudocapacitor, fuel cell, lithium ion batteries, water splitting and energy applications. It is well documented in the literature that the pseudocapacitive performance of oxides depends on many factors such as type of oxide, surface area and morphology, electrolyte, temperature etc. In view of this, the present work delineates efforts to understand the effect of morphology on the electrocapacitive behavior of Co_3O_4 nanostructured particles. The systematic morphological changes in Co_3O_4 is achieved by varying hydrolyzing agent, urea content during the hydrothermal synthesis of particles. Morphology and size analysis using scanning electron microscopy (SEM), show hierarchical structures namely plate like architecture and brush like structures of particles. The electrochemical measurements are performed using standard three-electrode system with 3M KOH electrolyte via cyclic voltammetry and galvanostatic charge-discharge methods. Amongst the Co_3O_4 studied, Co_3O_4-U0.37 displayed moderate surface area (50.10 m^2/g), highest specific capacitance (764 F/g at 5mV/s) and energy density (19.56 Wh/kg). The specific capacitance of all Co_3O_4 decreased with the increase in scan rate. The cyclic stability of Co_3O_4-U0.37 is studied up to 5,000 cycles and about 64% retention in charge storage capacity was observed. The superior electro-capacitive behavior of the Co_3O_4-U0.37 is attributed to high surface area, brush like structure, and high electrical conductivity amongst studied Co_3O_4. In conclusion, it is demonstrated that high specific capacitance is achievable in the same oxide material by the tight control of morphology of the material. The low hydrolyzing concentration aided in producing high surface area architecture.

TABLE OF CONTENTS

LIST OF TABLES

LIST OF FIGURES

CHAPTER 1

INTRODUCTION

1.1 Energy storage

Why store energy, and in particular, why store electrical energy? Energy storage is a critical component of manufacturing, of the service industry, of the future renewable energy industry, and of all the portable electronics with which we have become obsessed. Without modern energy storage, using lithium-ion (Li-ion) batteries, the decade of the smartphone, iPad, and iPod would not have progressed as it did [1]. Besides entertainment, energy storage plays a critical role in high-tech manufacturing where it is essential to have an uninterruptable power source of constant frequency. It is reported that some $80 billion is lost by U.S. industry [2] each year because of mainly short power interruptions. To ameliorate this, high-tech high-cost industry such as chip fabs have large power storage backups, using, for example, lead acid batteries, as well as frequency smoothing. Flywheels and ultracapacitors are finding application for grid frequency regulation in such critical applications, as utilities commonly vary the frequency to smooth the power output. Some essential service industries, such as the telephone industry rely mainly on large batteries for backup in case of power failure. In remote areas, such as Fairbanks, Alaska, a 40-MW Ni/Cd battery system is used to guarantee continuous power availability. There is a great need for electrical energy storage, not only for mobile electronic devices, such as cell phones, computers, and iPods, but also for transportation and load-leveling and for the effective commercialization of renewable resources such as solar and wind power. **Fig.1.1** shows a typical renewable energy generation system with energy storage.

Much attention is being given to hybrid electric vehicles (HEVs), in which batteries and/or capacitors are used to capture the energy evolved in braking. A related application is the

capture of the energy normally wasted when a dock crane is lowering a crate; capturing this energy through capacitors saves around 40% of total energy utilization. Similarly, subway trains, with many stops and starts, can capture the braking energy entering the station for use in accelerating out of the station. The next generation of electric vehicles might be plug-in hybrids, in which larger batteries are used and the vehicle can be recharged by plugging into the electrical power line. An effective unlimited range can be attained by using a small internal engine as a battery charger; the waste heat from the internal combustion engine can provide the heating and defogging energy. The all-electric vehicle might find a few niche markets; these include city buses and postal delivery and utility repair vehicles with much stopping and starting and limited daily ranges, high-cost hot-rod sports cars, and small commuter cars. In all of these transportation applications, low cost and long life are essential for commercial success. Neither can be attained with the present chemical storage battery and capacitor charge storage systems [3].

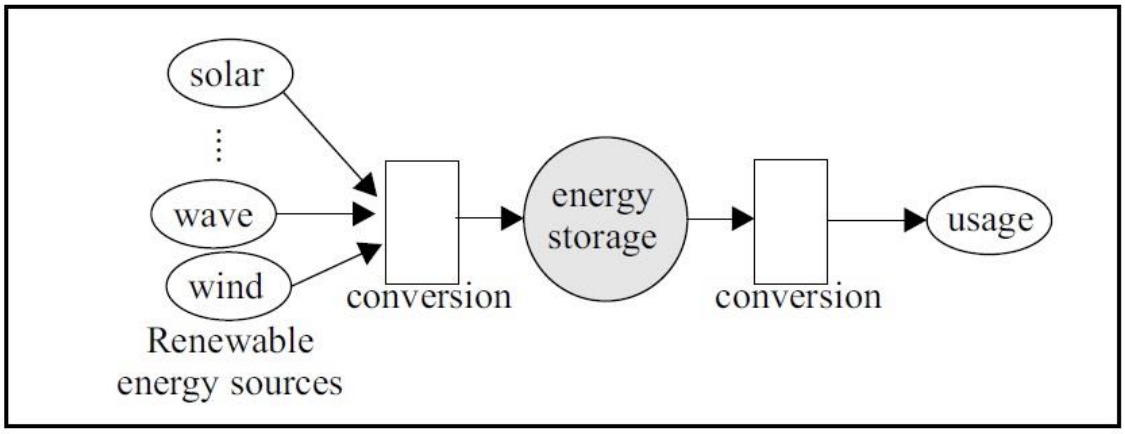

Fig.1.1. A typical renewable (distributed) energy generation system with energy storage [4].

Renewable energy sources are highly variable and un-predictable in their power output. To smoothen out this intermitted supply of energy, an energy storage device can be used. This device is charged when a surplus of energy is available, and discharged when the source does not

produce enough power for the load. Broadly two classes of energy storage can be identified, based on the length of the power transfer interval: short-term and long-term power transfer. The situation described above, where an energy storage device acts as an energy buffer, falls under long-term power transfer. Power can be delivered in this case from a few seconds to a few minutes or even longer. Short-term power transfer would for example be used to protect sensitive equipment against momentary voltage sags. In this case, power transfer can take place from a few milliseconds to a few seconds. In many cases, a short voltage sag can be ridden through with- out energy storage by making use of appropriate techniques [5].

1.2 Purpose of energy storage

Energy storage is the storage of some form of energy that can be drawn upon later to perform some useful operation. All forms of energy are either potential energy, chemical or gravitational energy:

i) A wind up clock stores potential energy (in this case mechanical, in the spring tension);

ii) A battery stores readily convertible chemical energy to keep a clock chip in a computer running even when the computer is turned off; and

iii) A hydroelectric dam stores power in a reservoir as gravitational potential energy.

Energy storage became a dominant factor in economic development with the widespread introduction of electricity and refined chemical fuels, such as gasoline, kerosene and natural gas in the late 1800s. Unlike other common energy storage used in prior use, such as wood or coal, electricity must be used as it is generated. Electricity is transmitted in a closed circuit, and for essentially any practical purpose cannot be stored as electrical energy. This meant that changes

in demand could not be accommodated without either cutting supplies (e.g., blackouts) or arranging for a storage technique [6].

The rapidly growing commercial markets providing portable electronic devices and other related electronics such as electric vehicles requires high-performance energy-storage systems [7].There is of course global issues threatening the environmental resulting in academics and industry exploring clean alternative energies where electricity storage needs to be either stored as electricity or in other forms of energy to meet growing consumers' needs [8]. Electrochemical supercapacitors (ECs), also called supercapacitors or ultracapacitors, are electronic components that can be rapidly charged and discharged and relied upon to store energy reliably for long periods. Emerging as an ideal model, they have been touted as a solution to the mismatch between the fast growth in power required by devices and the inability of batteries in various applications which require transient but high/peak power pulses for the time-dependent usage [9].

1.3 Energy storage methods

1.3.1 Chemical energy storage

Chemical fuels have become the dominant form of energy storage, both in electrical generation and energy transportation. Chemical fuels in common use are processed coal, gasoline, diesel fuel, natural gas, liquefied petroleum gas (LPG), propane, butane, ethanol, biodiesel and hydrogen. All of these chemicals are readily converted to mechanical energy and then to electrical energy using heat engines that used for electrical power generation.

Hydrogen: Hydrogen is a chemical energy carrier, just like gasoline, ethanol or natural gas. The unique characteristic of hydrogen is that it is the only carbon-free or zero-emission

chemical energy carrier. Hydrogen is a widely used industrial chemical that can be produced from any primary energy source.

Biofuels: Various biofuels such as biodiesel, straight vegetable oil, alcohol fuels, or biomass can be used to replace hydrocarbon fuels. Various chemical processes can convert the carbon and hydrogen in coal, natural gas, plant and animal biomass, and organic wastes into short hydrocarbons suitable as replacements for existing hydrocarbon fuels.

1.3.2 Electrochemical energy storage

An early solution to the problem of storing energy for electrical purposes was the development of the battery, an electrochemical storage device. It has been of limited use in electric power systems due to small capacity and high cost.

Batteries: A battery is a device that transforms chemical energy into electric energy. All batteries have three basic components in each cell – an anode, a cathode, and an electrolyte and their properties relate directly to their individual chemistries. Batteries are broadly classified into primary and secondary.

Fuel Cells: Fuel cells were invented about the same time as the battery. However, fuel cells were not well developed until the advent of space-crafts when lightweight, non-thermal sources of electricity were required. Fuel cell development has increased in recent years to an attempt to increase conversion efficiency of chemical energy stored in hydrocarbon or hydrogen fuels into electricity. Like a battery, a fuel cell uses stored chemical energy to generate power. Unlike batteries, its energy storage system is separate from the power generator. It produces electricity from an external fuel supply as opposed to the limited internal energy storage capacity of a battery [10].

1.3.3 Electrical energy storage

Superconducting magnetic energy storage (SMES): In a SMES system, energy is stored within a magnet that is capable of releasing megawatts of power within a fraction of a cycle to replace a sudden loss in line power. It stores energy in the magnetic field created by the flow of direct current (DC) power in a coil of superconducting material that has been cryogenically cooled [11].

Capacitor: Capacitors are two-terminal electrical elements. They are essentially two conductors, usually conduction plates - but any two conductors - separated by an insulator - a dielectric - with connection wires connected to the two conducting plates. They store energy on the surfaces of metalized plastic film or metal electrodes. When compared to batteries and supercapacitors, the energy density of capacitors is very low – less than 1% of a supercapacitor's, but the power density is very high, often higher than that of a supercapacitor. This means that capacitors are able to deliver or accept high currents, but only for extremely short periods, due to their relatively low capacitance [7].

Supercapacitor:A supercapacitor (sometimes ultracapacitor,formerly electric double layer capacitor (EDLC) is a high-capacity electrochemical capacitor with capacitance values much higher than other capacitors (but lower voltage limits) that bridge the gap between electrolytic capacitors and rechargeable batteries. They typically store 10 to 100 times more energy per unit volume or mass than electrolytic capacitors, can accept and deliver charge much faster than batteries, and tolerate many more charge and discharge cycles than rechargeable batteries. They are however 10 times larger than conventional batteries for a given charge. Energy storage is by means of static charge rather than of an electrochemical process inherent to the battery. Supercapacitors rely on the separation of charge at an electrified

interface that is measured in fractions of a nanometer, compared with micrometers for most polymer film capacitors.

The lifetime of supercapacitors is virtually indefinite and their energy efficiency rarely falls below 90% when they are kept within their design limits. Their power density is higher than that of batteries while their energy density is generally lower. However, unlike batteries, almost all of this energy is available in a reversible process.

1.4 Introduction to capacitor

Conventional capacitors consist of two conducting electrodes separated by an insulating dielectric material. When a voltage is applied to a capacitor, opposite charges accumulate on the surfaces of each electrode. The charges are kept separate by the dielectric, thus producing an electric field that allows the capacitor to store energy. This is illustrated in Figure **Fig.1.2.**

Capacitance C is defined as the ratio of stored (positive) charge Q to the applied voltage V:

$$C = \frac{Q}{V} \tag{1}$$

For a conventional capacitor, C is directly proportional to the surface area A of each electrode and inversely proportional to the distance D between the electrodes:

$$C = \varepsilon \frac{A}{D} \tag{2}$$

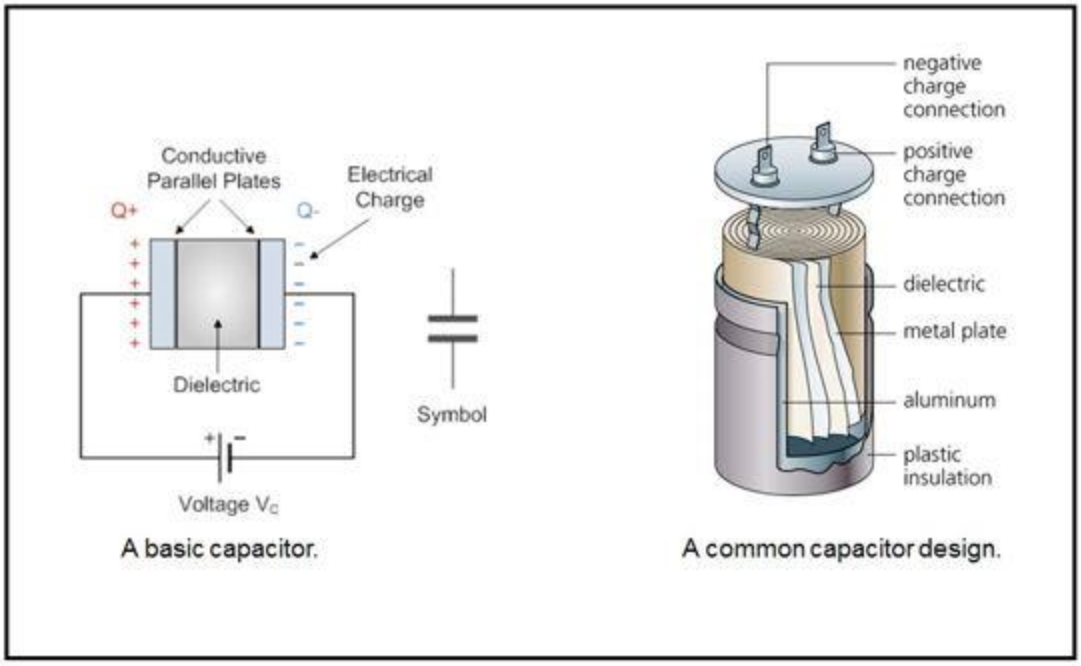

Fig.1.2. Schematic of a supercapacitor [12].

Where $\mathcal{E} = \varepsilon_0 \varepsilon_r$ is a constant of proportionality wherein ε_0 is the dielectric constant (or "permittivity") of free space and ε_r is the dielectric constant of the insulating material between the electrodes.

The two primary attributes of a capacitor are its energy density and power density. For either measure, the density can be calculated as a quantity per unit mass or per unit volume. The energy E stored in a capacitor is directly proportional to its capacitance:

$$E = \frac{1}{2} CV^2 \tag{3}$$

In general, the power P is the energy expended per unit time. To determine P for a capacitor, though, one must consider that capacitors are generally represented as a circuit in series with an external "load" resistance R, as is shown in **Fig.1.2.**

The internal components of the capacitor (e.g., current collectors, electrodes, and dielectric material) also contribute to the resistance, which is measured in aggregate by a quantity known as the equivalent series resistance (ESR). These resistances determine the

voltage during discharge. When measured at matched impedance (R = ESR), the maximum power P_{max} for a capacitor is given by:

$$P_{max} = \frac{V^2}{4 \times ESR} \quad (4)$$

This relationship shows how the ESR can limit the maximum power of a capacitor.

Conventional capacitors have relatively high power densities, but relatively low energy densities when compared to electrochemical batteries and to fuel cells. That is, a battery can store more total energy than a capacitor, but it cannot deliver it very quickly, which means its power density is low. Capacitors, on the other hand, store relatively less energy per unit mass or volume, but what electrical energy they do store can be discharged rapidly to produce a lot of power, so their power density is usually high.

Supercapacitors are governed by the same basic principles as conventional capacitors. However, they incorporate electrodes with much higher surface areas A and much thinner dielectrics that decrease the distance D between the electrodes. Thus, from Equations 2 and 3, this leads to an increase in both capacitance and energy.

Furthermore, by maintaining the low ESR characteristic of conventional capacitors, supercapacitors also are able to achieve comparable power densities. Additionally, supercapacitors have several advantages over electrochemical batteries and fuel cells, including higher power density, shorter charging times, and longer cycle life and shelf life. **Fig. 1.2** provides a schematic diagram of a supercapacitor.

The performance improvement for a supercapacitor is shown in **Fig.1.3** graph termed a "Ragone plot." This type of graph presents the power densities of various energy storage devices, measured along the vertical axis, versus their energy densities, measured along the horizontal axis. In **Fig.1.3**, it is seen that supercapacitors occupy a region between conventional capacitors

and batteries. Despite greater capacitances than conventional capacitors, supercapacitors have yet to match the energy densities of mid to high-end batteries and fuel cells. Thus, much of the literature surveyed for this overview focuses on developing improved types or classes of supercapacitors to make their energy densities more comparable to those of batteries. These factors and trends are reflected in the taxonomy of supercapacitors presented in the next section.

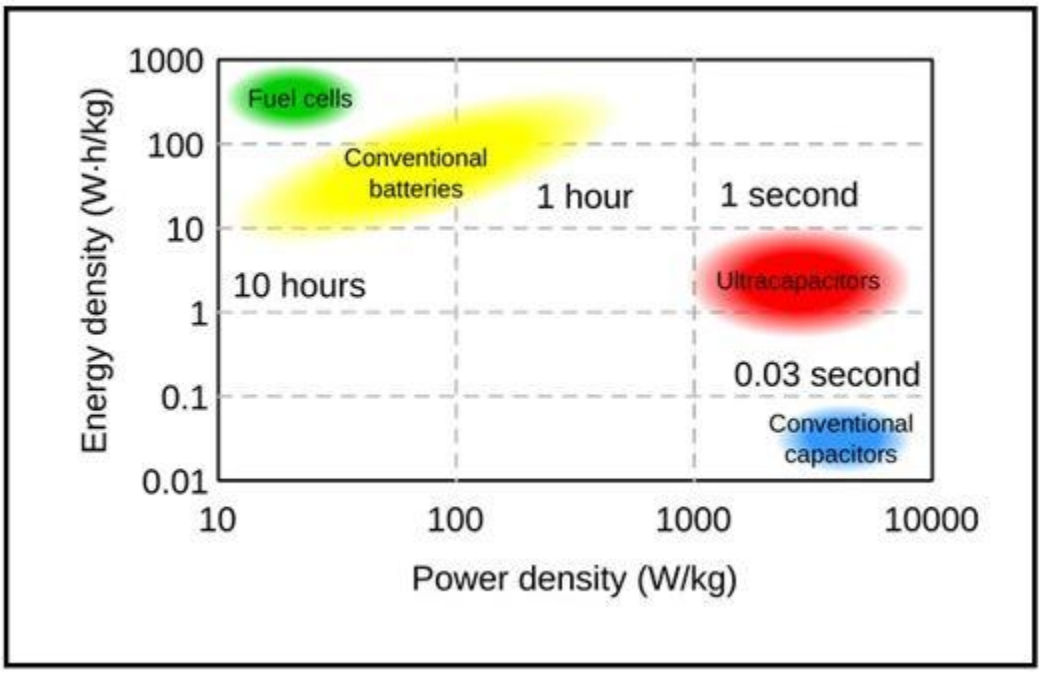

Fig.1.3. Comparison of energy density and power density for various energy storage devices [13].

1.5 Comparison of supercapacitors and batteries

While batteries and capacitors have similarities, there are several key differences. **Table 1.1** shows the differences of performance of supercapacitors and batteries. The potential energy in a capacitor is stored in an electric field, where a battery stores its potential energy in a chemical form. The technology for chemical storage currently yields greater energy densities (capable of storing more energy per weight) than capacitors. However, when a battery is discharging it can be slower than a capacitor ability to discharge because there is a latency associated with the chemical reaction to transfer the chemical energy into electrical energy. A

capacitor is storing the electrical energy directly on the plates so discharging rate for capacitors are directly related to the conduction capabilities of the capacitors plates. A capacitor is able to discharge and charge faster than a battery because of this energy storage method. But unlike a battery that can turn its electrical current on and off, once a capacitor is connected to an outside circuit it will discharge as fast as it can until all the charge is drained.

Table.1.1. PERFORMANCE COMPARISION BETWEEN SUPERCAPACITOR AND LI-ION BATTERIES [14].

Function	Supercapacitor	Lithium-ion
Charge time	1-10 seconds	10-60 minutes
Cycle life	1 million or 30,000h	500 and higher
Cell voltage	2.3 to 2.75 V	3.6 to 3.7 V
Specific energy (Wh/kg)	5 (typical)	100-200
Specific power (W/kg)	Up to 10,000	1,000 to 3,000
Cost per Wh	$20 (typical)	$0.50-$1.00 (large system)
Service life (in vehicle)	10 to 15 years	5 to 10 years
Charge temperature	-40 ºC to 65 ºC	0 ºC to 45 ºC
Discharge temperature	-40 ºC to 65 ºC	-20 ºC to 60 ºC

1.5 Supercapacitors

Because of increasing demand of power in the modern society, energy storage/consumption is playing a more important role on future economics. The reliance on fossil fuels such as petroleum however has a severe impact on the global ecology. Therefore, energy storage systems that are more environmentally friendly, low-cost and high-performance have attracted much attention [15]. Electrochemical energy storage/conversion system with the mentioned properties is a prominent candidate for the modern energy storage systems.

Electrochemical energy storage systems can be divided into three categories, which are batteries, fuel cells and supercapacitors, based on different energy conversion mechanisms. The

common denominators that the systems share are the separated electron/ion transport and that the energy conversion process happens at the electrode/electrolyte interface [9].

In batteries and fuel cells, energy is stored in the form of chemical energy and is converted to electrical energy through redox reactions. Cathode, anode and electrolyte are the common components in both battery and fuel cell. Ionic conductivity is provided by electrolytes, which eventually allows electric charges move to move between two electrodes. **Fig.1.4** shows the schematic diagram of fuel cell.

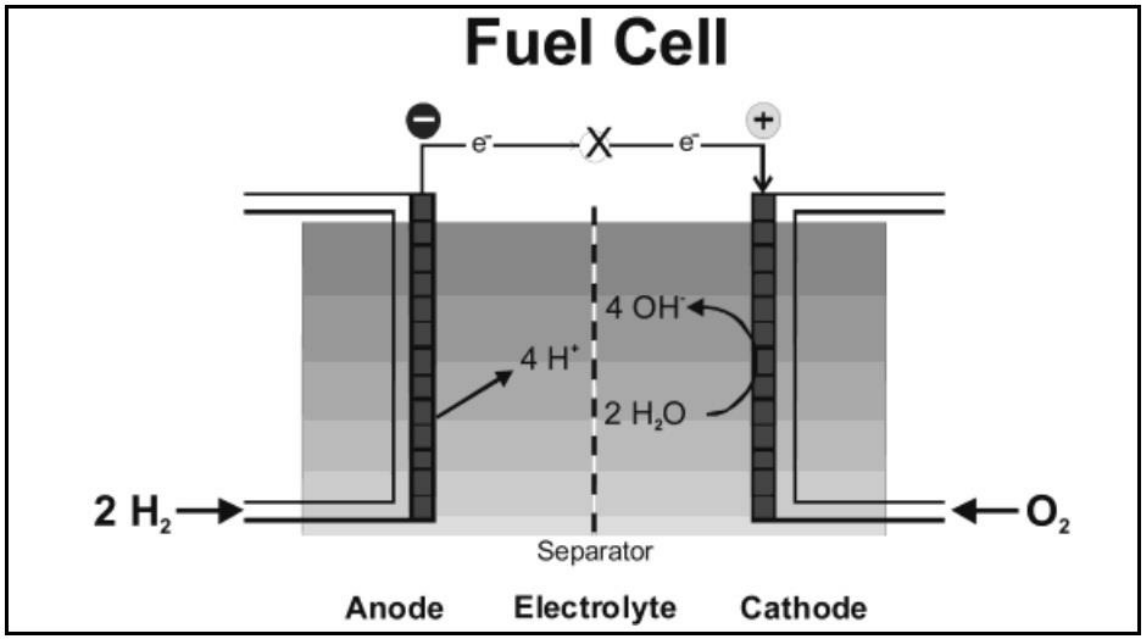

Fig.1.4. Schematic of a fuel cell [15].

The main difference between batteries and fuel cells is the locations where energy is stored [9]. In batteries, cathodes and anodes are the medium of charge-transfer and the places energy is stored. Electrodes are either reduced or oxidized, thus the redox reaction powers the battery. As a closed system, energy storage and conversion happen inside the system, which means chemical energy a battery carries is strictly limited to the electrode materials. On the contrary, fuel cells are open systems that require a constant source of chemical energy from outside the cell to run the reaction. Cathodes and anodes in fuel cells are just charge-transfer

media. Because of the character, fuel cells are capable of producing electricity continuously if inputs are supplied constantly from environment.

In supercapacitors, electric energy is stored at the electrode/electrolyte interface where an electrochemical double layer is formed [16]. Energy storage in the supercapacitors consists of electrostatic storage from separation of charge in a double layer at the electrode/electrolyte interface, and faradaic electrochemical storage from redox reactions.

An ideal energy storage system compromises high-energy capacity and high rate of energy conversion. The reason for the interest in development of different electrochemical energy storage systems is shown in **Fig.1.3**, the so-called "Ragone chart" [17]. It is a chart used for performance comparison of various energy storage and conversion devices. "specific energy" (Wh/kg) or "energy density" (Wh/L) are the terms used to describe the energy contents of a system, whereas the speed of charge/discharge is indicated by the "specific power" (Wh/kg) or "power density" (Wh/L). The variations between the electrochemical energy storage systems come from the different energy storage/conversion mechanisms.

Fuel cells have the highest specific energy in the Ragone chart, which is mainly because of the constant chemical energy source from outside. As the most widely used energy storage system, battery has a lower energy capacity compared to fuel cells. Capacitors can be considered as high power systems based on the charge/discharge mechanism. Supercapacitors occupy the area between batteries and conventional capacitors.

Supercapacitors have several orders of magnitude higher power density than that of battery, with a higher amount of energy stored compared to a conventional capacitor. Nevertheless, the amount of energy stored in supercapacitors is significantly lower than that of batteries and fuel cells.

Supercapacitor was demonstrated and patented by General Electric in 1957 [9]. Since then it has been attracting considerable attention from both scientists and engineers. With the features of longer cycle life, low maintenance, rapid charge/discharge and high power density, supercapacitors are believed to be capable of meeting the rapid growing demand for clean energy storage [18]. Nowadays, supercapacitors are used in a wide and growing range of high power density required applications.

Supercapacitors can be divided into two categories based on different energy storage mechanisms: electric double-layer capacitors (EDLCs) and pseudocapacitors [10]. **Fig.1.5** shows taxonomy of supercapacitors. EDLCs store energy using the adsorption of both anions and cations, and accumulated charge at electrode/electrolyte interface. So called "electric double-layer" refers to the layer of charge at the electrode/electrolyte interface that stores the charge. With the use of high surface area electrode materials significantly higher quantities of charge can be stored. Therefore, porous carbon materials with higher specific surface area and pore-size distribution, such as

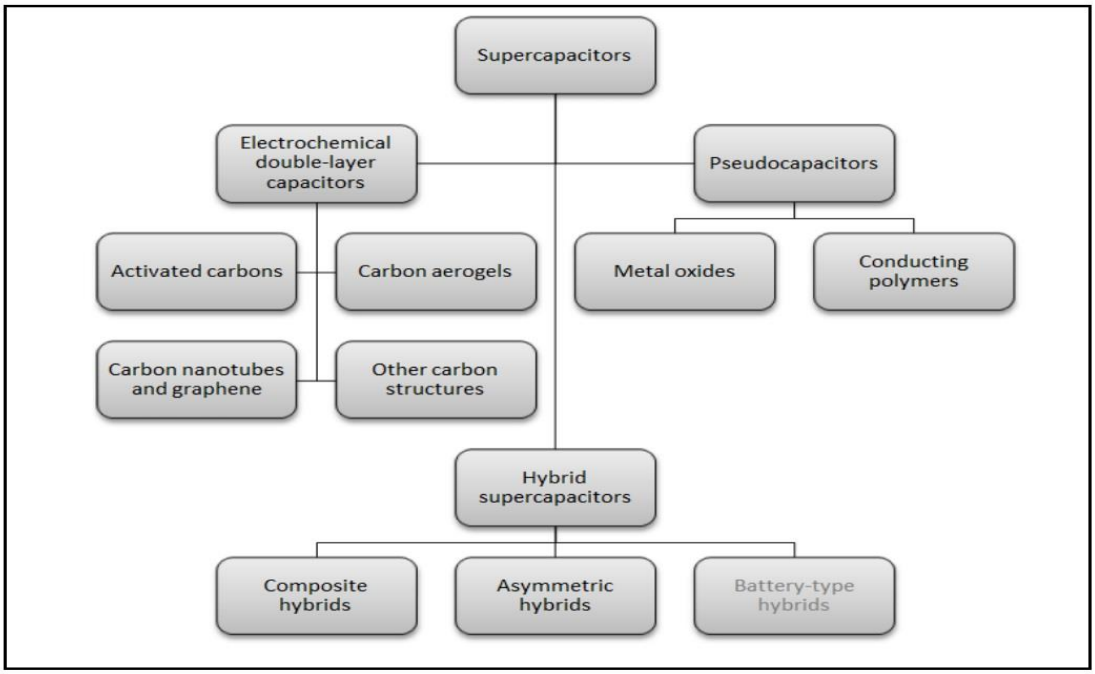

Fig.1.5. Taxonomy of Supercapacitors [19].

activated carbons, aerogels, CNTs and mesoporous carbons, have been studied for use as electrodes in EDLCs [10]. Because of electrostatic surface-charge accumulation, EDLCs have very high rates of charge/discharge and infinite lifetime in principles, which makes it environmentally friendly (**Fig. 1.6**).

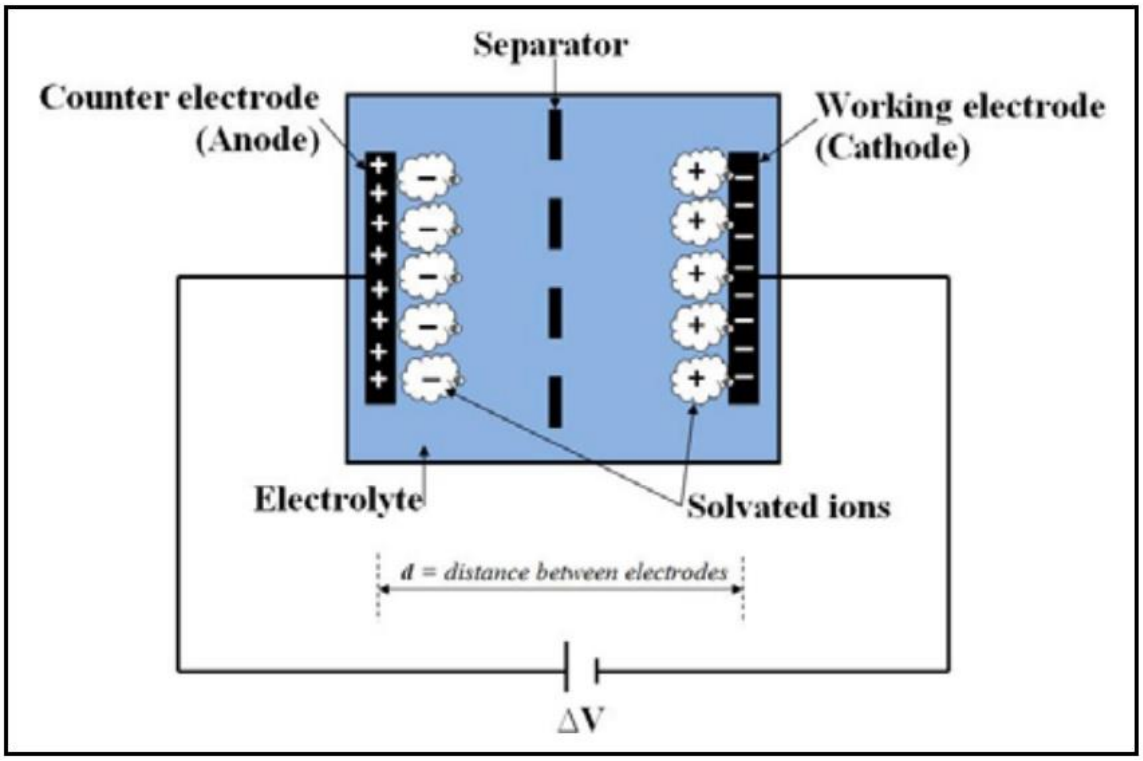

Fig.1.6. Schematic diagram of an electrochemical double-layer capacitor [20].

1.6 Pseudocapacitors

In contrast to EDLCs, that store charge electro-statically, pseudocapacitors store charge faradaically through the transfer of charge between electrode and electrolyte. This is accomplished through electrosorption, reduction-oxidation reactions, and intercalation processes [21,22,23].The pseudo-capacitors may be allowed to achieve greater capacitance properties and energy densities than EDLCs by presence of Faradaic processes [15,24]. Two types of electrode materials are served to store charge in pseudocapacitors: (i) metal oxides and (ii) conducting polymers.

1.6.1 Metal oxides

Because of their high conductivity, metal oxides viz. NiO, MnO_2, Fe_3O_4, Co_3O_4, $NiCo_2O_4$, RuO_2 etc. have also been explored as a possible electrode material for pseudocapacitors [10, 13, 25, 26, 27]. The majority of relevant research concerns ruthenium oxide. This is because other metal oxides have yet to obtain comparable capacitances. The capacitance of ruthenium oxide is achieved through the insertion and removal, or intercalation, of protons into its amorphous structure. In its hydrous form, the capacitance exceeds that of carbon-based and conducting polymer materials [20-21]. Furthermore, the ESR of hydrous ruthenium oxide is lower than that of other electrode materials. As a result, ruthenium oxide pseudocapacitors may be able to achieve higher energy and power densities than similar EDLCs and conducting polymer pseudocapacitors. However, despite this potential, the success of ruthenium oxide has been limited by its prohibitive cost. Thus, a major area of research is the development of fabrication methods and composite materials to reduce the cost of ruthenium oxide, without reducing the performance [10, 13, 19].

1.6.2 Conducting polymers

Conducting polymers have a relatively high capacitance and conductivity, plus a relatively low ESR and cost compared to carbon-based electrode materials [28]. In particular, the n/p-type polymer configuration, with one negatively charged (n-doped) and one positively charged (p-doped) conducting polymer electrode, has the greatest potential energy and power densities; however, a lack of efficient, n-doped conducting polymer materials has prevented these pseudocapacitors from reaching their potential [29].

1.7 Applications of pseudocapacitors

Electrochemical supercapacitors are still novel devices that have yet to practice widespread use. This is all because of their restricted power and energy capabilities, and therefore find only useful in low power and energy applications like memory backup. Currently, great advances have been made in improving characteristics like energy and power density. Novel applications for EDLCs are being discover and promoting at excellent rate [30]. The supercapacitors find application in electric vehicles, battery enhancement, memory backup, improved quality of power and many more.

1.8 Limitation of pseudocapacitors

The major advantages of using supercapacitor against batteries include extended life time, amplified rated voltage, wide range of working temperature, superior energy and power densities, excellent cyclability (hundreds of thousands charge/discharge cycles as compared with hundreds of cycles for storage batteries) [31]. However, like every device's limitation, supercapacitors too have some demerits like low energy density for example it generally holds 1/5th to1/10th of a battery. Inability to use the full energy spectrum for some applications. To get higher voltages, serial connections are required as these are low voltage cells. A voltage-balancing element is always required to connect more than three supercapacitors in series to use accordingly for any application. Disadvantage of self-discharge in compared to electrochemical batteries.

CHAPTER 2

LITERATURE REVIEW

2.1 RuO_2 pseudocapacitance

Most of the work on pseudocapacitors utilizing pseudo-capacitance has been done using mixed metal oxide materials, but the most success has been achieved using ruthenium and tantalum oxides [32,33]. The high cost of ruthenium has resulted in a search for other metal oxides and nitrides for use in pseudocapacitors electrodes, but no substitute for ruthenium has been found with a comparable specific capacitance and higher surface area [27]. The most extensive efforts to develop pseudocapacitors using ruthenium oxide have been done at Pinnacle Research Institute (PRI) [34,35]. The PRI devices utilized a thin 10–50 μm layer of ruthenium / tantalum oxide on a titanium substrate with sulfuric acid as the electrolyte.

Since the pioneering study by Trasatti and Buzzanca who first recognized that the 'rectangular' shaped cyclic voltammogram of a RuO_2 film resembled that of the electric double layer capacitors, much effort has been devoted to enhancing the capacitance as well as the fundamental understanding of the mechanism of the pseudocapacitance [36].They found the film of RuO_2 behaves as an electric condenser exhibiting a charging and discharging process in 1M $HClO_4$ at scan rate of 40 mV/s.

Gujar et.al. successfully electrochemically deposited ruthenium oxide (RuO_2) onto tin doped indium oxide (ITO) electrode and used as electrodes to form a supercapacitor in a 0.5M H_2SO_4 electrolyte [37]. For electrochemical supercapacitor applications, He found that the electrochemically prepared crystalline RuO_2 was stable for large number of cycles with the specific capacitance 498 F/g at a scan rate of 5 mV/s. He also observed that the specific

capacitances of RuO_2 electrode decreased with an increase of scan rate and maximum capacitance 498 F/g was observed at 5 mV/s.

Zheng et.al. demonstrated an excellent electrode property of $RuO_2.xH_2O$ be an excellent electrode material for electrochemical capacitors as prepared by a sol-gel process at low temperatures and found that specific capacitance is over 720 F/g [38]. This value is at least two times higher than the highest value ever reported for such materials.

Bi et.al. investigated RuO_2 nanoparticles on carbon nanotubes for potential application in electrochemical capacitors as electrode materials [39]. He demonstrated that the supporting material of carbon nanotubes can significantly promote the supercapacitance performance of RuO_2 and achieved a specific capacitance as 953 F/g. The results presented give clear evidence of the ability of CNTs to improve the electrochemical performance of electrode materials, such as nanostructured transition metal oxides.

Provencher et.al. reported for the first time that pseudocapacitance can arise on a metal oxide electrode (RuO_2) in a PIL electrolyte composed of 2-methylpyridine and trifluoroacetic acid [40].He also studied the capacitive behavior on a thermally prepared RuO_2 electrode of several new protic ionic liquids composed of heterocyclic amines and trifluoroacetic acid (TFA) at the 1:1 and 1:2 base: acid ratio where he found the Redox peaks attributed to the shift of the oxidation state of RuO_2, thus giving direct evidence that pseudocapacitance is involved in the energy storage mechanism.

Hu et.al. successfully designed and tailored an advanced electrode material with a 3D, arrayed, nanotubular architecture; annealed $RuO_2.xH_2O$ nanotubes which achieve the performances (ultrahigh-power characteristics and high capacity) required for next generation supercapacitors by using a very simple, one-step, reliable, cost-effective, anodic deposition

technique [41]. This unique structure not only reduces the diffusion resistance of electrolytes but also enhances the facility of ion transportation and maintains the very smooth electron pathways for the extremely rapid charge/discharge reactions. The specific power and specific energy of $RuO_2.xH_2O$ nanotubular arrayed electrodes is equal to 4320 kW /kg and 7.5 W h/kg, respectively, achieving the perfect performance for next generation supercapacitors where specific capacitance was found as 740 F/g.

Chen et.al. developed a simple and efficient approach to produce hybrid nanostructured electrodes via the integration of RuO_2 nanowires and printed single-walled carbon nanotube films [42] which displayed an enhanced device performance, in terms of coulombic efficiency of >99%, specific capacitance of 138 F/g, power density of 96 kW/kg, and energy density of 18.8 Wh/kg suggesting that printable electrochemical capacitors hold significant promise for applications in wearable energy storage devices, and can be fully integrated with the fabrication process in current printed electronics.

Liu et.al. successfully prepared a series of $Co_3O_4/RuO_2{\cdot}xH_2O$ by one-step co-precipitation method with the usage of P123 as a soft template [43]. From the results of electrochemical measurements, he found that the specific capacitances and stability of the composites are strongly dependent on the heat treatment temperature. A highest capacitance of 642 F/g was obtained from the composite with molar ratio of Co:Ru = 1:1 at 150 ˚C and the capacitance gradually decrease with rising of the heat treatment temperature ranging from 150 ˚C to 900 ˚C, but the recyclability of the composites is improved.

Among the transition-metal oxides, ruthenium oxide has been employed as one of the most important electrode materials for electrochemical supercapacitors because of its ultrahigh pseudocapacitance and reversibility of accepting and donating protons from an aqueous

electrolyte. The above synthesis methods gave improvement of specific capacitance of RuO_2 to some extent. However, because of the high cost of Ruthenium, the commercial application of RuO_2 as electrode materials in supercapacitors has been restricted. The limitation has encouraged several studies of cheap metal –oxides.

2.2 Supercapacitance in metal-oxides

Supercapacitors using metal oxides for the electrodes has been under development for nearly ten years. Most of the work has been done using ruthenium oxides, but more recently other metal oxides have received attention in order to use precursor materials for electrode formation that are more plentiful and lower cost than ruthenium oxides. Extensive efforts have been devoted to improve the specific capacitance of supercapacitors by introducing pseudo-capacitive metal oxides. Compared with EDLC-based capacitors; pseudocapacitor based on metal oxide electrodes have attracted a large amount of attention since they can produce higher capacitances than double-layer carbonaceous materials. In terms of base metal oxides such as MnO_2, NiO, Fe_3O_4, etc., their outstanding pseudo-capacitive behavior, practical availability, environmental compatibility and lower cost have been demonstrated when compared to the state-of-the-art supercapacitor material RuO_2.

Zhang et.al. reported a facile way to grow various porous NiO nanostructures including nanoslices, nanoplates, and nanocolumns, which show a structure-dependence in their specific charge capacitances [44]. The formation of controllable porosity was due to the dehydration and re-crystallization of β-$Ni(OH)_2$ nanoplates synthesized by a hydrothermal process. The specific capacitance of the porous NiO nanocolumns (390 F/g) is significantly higher than that of the nanoslices (176 F/g) or nanoplates (285 F/g) at a discharge current of 5 A/g. This approach provides a clear illustration of the process–structure–property relationship in nanocrystal

synthesis and potentially offers strategies to enhance the performance of supercapacitor electrodes.

Nam et.al. prepared NiO_x thin film electrodes for use in a supercapacitor by electrochemical precipitation of $Ni(OH)_2$ films followed by heat-treatment [45]. He examined the effect of electrodeposition conditions such as cathodic current density and concentration of $Ni(NO_3)_2$ solution on the surface morphology of NiO_x and found to have a significant effect on the surface morphology of the deposited films. A maximum specific capacitance of 277 F/g was obtained for a highly porous NiO_x film electrode prepared by heating the $Ni(OH)_2$ film deposited at 4.0 mA/cm^2 in 0.1 M $Ni(NO_3)_2$ at 300 $^{\circ}C$ which seems to be caused by an increase in the surface active sites, which is induced by the formation of a porous surface morphology.

Pang et.al. deposited thin films of manganese dioxide on nickel foils by electrodeposition and by both dip-coating and drop-coating with manganese dioxide suspensions (sols) and their subsequent gelation and calcination [46]. The performance of these films as ultracapacitors was studied by cyclic voltammetry in the range 0.0-0.9 V (SCE) and by chronopotentiometry in unbuffered Na_2SO_4 solution. The cyclic voltammograms of ultrathin, dip-coated sol-gel-derived films indicated better capacitive behavior and gave differential specific capacitance values as high as 698 F/g compared to values half to two-thirds as great for the electrodeposited films. In conclusion, sol-gel-derived nano particulate manganese dioxide thin films on nickel foils have been shown to be an outstanding electrode material for the fabrication of ultracapacitors.

Chen et.al. fabricated flexible asymmetric supercapacitors (ASCs) based on transition-metal-oxide nanowire/single-walled carbon nanotube (SWNT) hybrid thin-film electrodes which exhibited a superior device performance with specific capacitance of 184 F/g, energy density of 25.5 Wh/kg, and columbic efficiency of 90% [47]. In this research, manganese dioxide

nanowire/SWNT hybrid films worked as the positive electrode, and indium oxide nanowire/SWNT hybrid films served as the negative electrode in a designed ASC. The superior performance was attributed to the enhanced charge storage contributed by electrical double-layer capacitance from SWNT films and pseudocapacitance from transition-metal oxide nanowires, and good conductivity as a result of using SWNTs as conductivity agent.

Du et.al. assembled and characterized activated carbon (AC)-Fe_3O_4 nanoparticles asymmetric supercapacitor cells in 6 M KOH aqueous electrolyte for the first time where the nanostructure Fe_3O_4 was prepared by the microwave method [48]. The supercapacitor delivered a specific capacitance of 37.9 F/g at a current density of 0.5 mA/cm^2. The result of cyclic characteristic test showed that it also could keep 82% of initial capacity over 500 cycles. The results of CV, EIS, and the charge/discharge measurements proved that this kind of hybrid supercapacitor has good electrochemical capacitance performance within potential range from 0 to 1.2 V.

Metal oxides used as electrode active materials for ECs have developed at a high rate over the past decades and may be classed as either noble or based metal oxides. However, their relatively high cost, low capacitance values and potential (reported) harmful nature to the environment have limited their widespread application in supercapacitors.

2.3 Supercapacitance in mixed metallic oxides

A promising family of mixed transition-metal oxides (MTMOs) (designated as $A_xB_{3-x}O_4$; A, B = Co, Ni, Zn, Mn, Fe, etc.) with stoichiometric or even non-stoichiometric compositions, typically in a spinel structure, has recently attracted increasing research interest worldwide. Benefiting from their remarkable electrochemical properties, these MTMOs will play significant roles for low-cost and environmentally friendly energy storage/conversion technologies.

Yuan et.al. fabricated an advanced three-dimensional electrode by growing ultrathin mesoporous $NiCo_2O_4$ nanosheets on Ni foam with strong adhesion for high-performance electrochemical capacitors [49]. The synthesis involved the co-electrodeposition of a bimetallic (Ni, Co) hydroxide precursor on a Ni foam support and subsequent thermal transformation to spinel mesoporous $NiCo_2O_4$. As a result, superior pseudocapacitive performance was achieved with an ultrahigh specific capacitance of 1450 F/g, even at a very high current density of 20 A/g, and excellent cycling performance at high rates, suggesting its promising application as an efficient electrode for electrochemical capacitors.

Cheng et.al. deposited $ZnCo_2O_4$ nanoflakes on a cellular nickel foam using a cost effective hydrothermal procedure where he found an excellent specific capacitance of 1220 F/g at a current density of 2 A/ g in a 2 M KOH aqueous solution and a long-term cyclic stability of 94.2% capacitance retention after 5000 cycles [50]. The mesoporous $ZnCo_2O_4$ nanoflakes have large electroactive surface areas with strong adhesion to the Ni foam, allowing fast ion and electron transport. The fabrication strategy is facile, cost-effective, and can offer great promise for large-scale supercapacitor applications. This may be due to the unique three-dimensional mesoporous nanoflakes architecture with a very large surface area and porosity offers faster ion/electron transfer, an improved reactivity and enhanced electrochemical kinetics.

Mondal et.al. successfully synthesized the mesoporous flake-like manganese-cobalt composite oxide ($MnCo_2O_4$) through the hydrothermal method [51]. As an electrode material for supercapacitors, the flake like $MnCo_2O_4$ also demonstrates a high supercapacitance of 1487 F/g at a current density of 1 A/g, and an exceptional cycling performance over 2000 charge/discharge cycles. In view of its simple preparation process and excellent electrochemical performance, this mesoporous flake like $MnCo_2O_4$ might serve as an attractive candidate for

LIBs and supercapacitors. The excellent electrochemical performance might be attributed due to the pores in the flake-like $MnCo_2O_4$, which not only serve as a reservoir for the electrolyte, but also enhance the diffusion kinetics in the interior of the electrode.

Wang et.al. successfully synthesized multi-shelled $CoFe_2O_4$ hollow microspheres with a tunable number of layers (1–4) via a facile one-step hydrothermal method using cyclodextrin as a template, followed by calcination at 550 ˚C for 2 hours [52]. The $CoFe_2O_4$ hollow spheres displayed significantly enhanced electrochemical performance relative to the reported $CoFe_2O_4$ nanocomposites because of the unique, porous, hollow multi-shelled structure. The initial capacities of the single-, double-, triple-, and quadruple-shelled $CoFe_2O_4$ microspheres were 406.8, 552.8, 1,450.0, and 1,211.0 F/g, respectively. This may be caused by activation of the electrode materials during the reaction. In addition, high capacitance of the $CoFe_2O_4$ hollow spheres may be attributed not only to the Faradic pseudocapacitance of the $CoFe_2O_4$ nanoparticles, but also to the unique structure of these nanocomposites.

While reviewing different literatures, it was well known that structures also character electrode materials. Due to the fact that the functionalities of materials can be tuned efficiently through manipulating their structures, diverse strategies have been developed successfully to produce materials with well-defined structures. Crystallographic nature may play important role in order to improve further the performances of energy storage devices such as supercapacitors.

2.4 Crystallographic structures of Co_3O_4

There has been an increasing interest in developing materials based on cobalt oxides because of their potential application in many technological fields [53].Co_3O_4 belongs to the normal spinel crystal structure based on a cubic close packing array of oxide ions.Co_3O_4 is one of the most intriguing magnetic p-type semiconductors known, and has found use in applications

in many fields, such as sensors, heterogeneous catalysts, electronic devices , magnetic materials, supercapacitors and solid state sensors [54]. Co_3O_4 crystallizes in the cubic normal spinel structure (space group $Fd\bar{3}m$) which contains cobalt ions in two different oxidation states, Co^{2+} and Co^{3+}. These are located at the interstitial tetrahedral (8a) and octahedral (16d) sites, respectively, of the close-packed face centered cubic (fcc) lattice formed by the oxygen ions. (**Fig.2.1**)

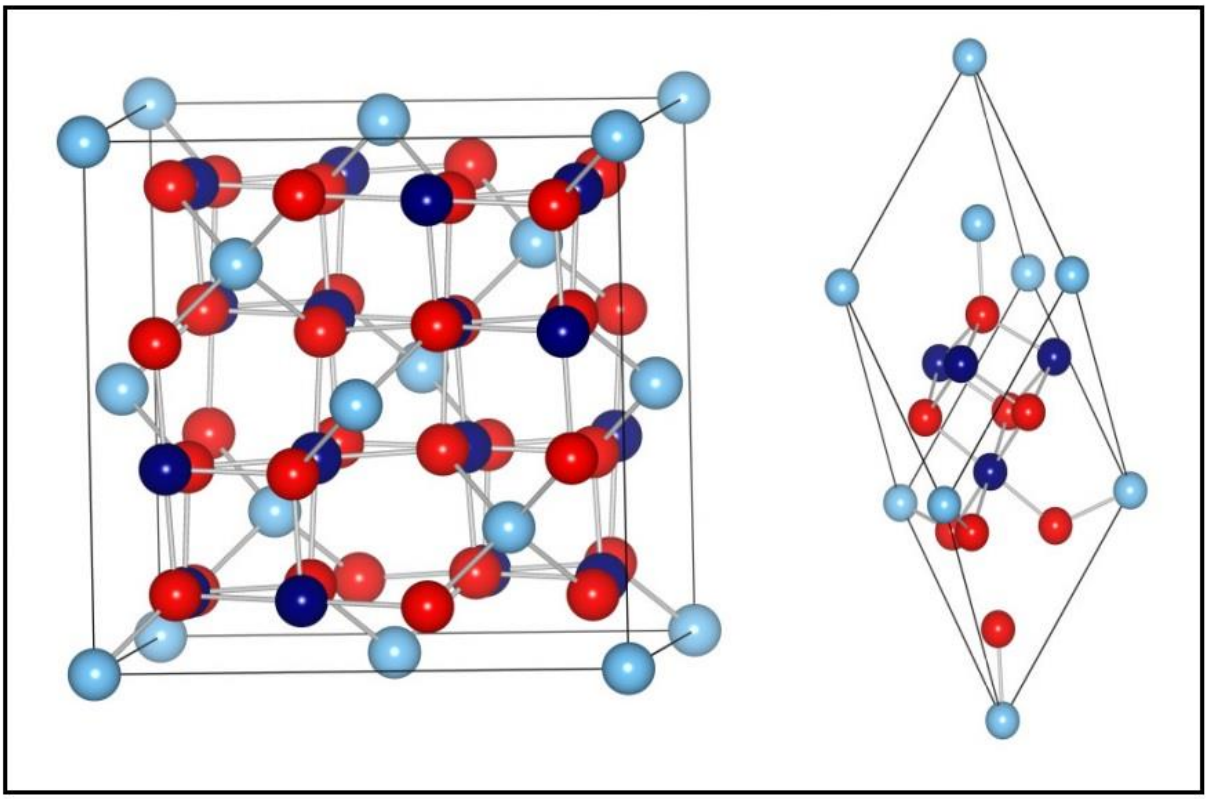

Fig.2.1. Unit cell (on the left) and primitive cell (on the right) of Co_3O_4. Light cyan and navy blue balls indicate Co^{2+} and Co^{3+} ions, red ones indicate O^{2-} ions [55].

In a simplified picture, the crystal fields at the 8a and 16d sites split the five degenerate atomic d orbitals into two groups, leading to 3 unpaired d electrons on Co^{2+}, while all the d electrons of Co^{3+} are paired **(Fig.2.2**). As a result, the Co^{3+} ions are not magnetic, whereas the Co^{2+} ions carry a magnetic moment. Experimentally, Co_3O_4 is a paramagnetic semiconductor at room temperature. It becomes antiferromagnetic below $T_N \sim 40$ K, [56] where the

antiferromagnetism is mainly due to the weak coupling between nearest neighbor Co^{2+} ions. The conductivity is usually p-type at low temperature and intrinsic at high temperature [57] measured values of the band gap are around 1.6 eV [58,59].

2.5 Co_3O_4 as supercapacitors

For the purpose of improving supercapacitors energy densities, numerous efforts have been made to investigate pseudocapacitive transition metal oxides or hydroxide (such as RuO_2, MnO_2, NiO, Co_3O_4, $Ni(OH)_2$, $Co(OH)_2$, $NiCo_2O_4$ etc.) and their composites with conductive additives, which could produce higher specific capacitance than typical carbonaceous materials with electric double layer capacitance. Among these available pseudocapacitive materials, Co_3O_4 is particularly attractive for application in supercapacitors, due to its low cost, low environmental footprint, great redox activity and especially, extremely high theoretical specific capacitance (3560 F/g) [60,61].

However, the observed specific capacitance for Co_3O_4 are much lower than its theoretical value [62], and it is still challenging and imperative to improve its specific capacitance as well as rate capability and long term stability with rational design and fabrication process.

2.6 Review of Co_3O_4 as electrode for supercapacitors

Gao et. al. successfully prepared Co_3O_4 nanowire arrays on nickel foam e prepared via template-free growth followed by thermal treatment at 300 ˚C in air, which showed a maximum specific capacitance of 746 F/g measured at a current density of 5 mA/cm^2 in KOH electrolyte solution [63].This excellent specific capacitance is due to the open spaces between neighboring nanowires which allow for easy diffusion of electrolyte into the inner region of the electrode, resulting in reduced internal resistance .In addition ,each nanowire has its own contact with the

nickel foam current collector ensuring all nanowires participate in the electrochemical reaction, and thus enhanced the utilization of active materials.

Wang et.al. synthesized nanoporous cobalt oxide nanorods using a facile and efficient hydrothermal method, nanoporous Co_3O_4 nanorods were prepared and maximum specific capacitance of 281 F/g was obtained at a 5 mV/s scan rate in 2 M KOH solution [64]. This indicated that the capacitance obtained was not pure double layer capacitance, but mainly originated from Faradaic pseudocapacitance. This high supercapacitance of Co_3O_4 nanorods could be attributed to the nanoporous structure of nanorods with high specific surface area.

Cui et.al. successfully synthesized Co_3O_4 nanorods by thermal decomposition of the precursor prepared via a facile and efficient microwave-assisted hydrothermal method, using cetyltrimethylammonium bromide (CTAB) with ordered chain structures as soft template for the first time [65]. This Co_3O_4 nanorods as electroactive materials for supercapacitor exhibited supercapacitance of 456 F/g for a single electrode even after 500 cycles, suggesting its potential application in electrochemical capacitors which could be due to the maximum charge transfer process at the electrode/electrolyte interface.

Shinde et.al. deposited uniform and adherent cobalt oxide thin films on glass substrates from aqueous cobalt chloride solution, using the solution spray pyrolysis technique and studied the possible application in energy storage devices using Co_3O_4 and found that the supercapacitor properties of spray deposited Co_3O_4 film is capable of exhibiting specific capacitance of 74 F/g [66] in 2M aqueous KOH electrolyte. This relatively low capacitance may be attributed to the anhydrous nature of Co_3O_4 electrode; due to high temperature preparation technique and the resistance of current collector, i.e. fluorine doped tin oxide (FTO) coated glass substrate.

Xu et.al. successfully synthesized Co_3O_4 nanotubes by chemically depositing cobalt hydroxide in anodic aluminum oxide (AAO) templates and thermally annealing at 500°C [62].The electrochemical capacitance behavior of the Co_3O_4 nanotubes electrode was investigated by cyclic voltammetry, galvanostatic charge–discharge studies and electrochemical impedance spectroscopy in 6 M KOH solution and demonstrated the good capacitive behavior with a specific capacitance of 574 F/g at a current density of 0.1 A/g which may be due to the surface adsorption of high concentration alkali ions which can decrease the electrolyte starvation near the electrode surface and reduce the internal resistance of the electrode, which help to improve the pseudocapacitance .

Wei et.al. successfully synthesized with the epoxide addition procedure for the first time by using cobalt nitrate as the precursor [67]. The specific capacitance of 623 F/g was observed, indicating high reversibility of the redox reaction on oxide surfaces. This high capacitance is due to increasing the difficulty for the diffusing electrolytes to access the internal pore surfaces of the porous electrode and increasing the pathway distances that the electrons need to travel. The high specific surface area and porosity as well as the mesoporous structure of the cobalt oxide aerogel are essential for the obtained outstanding supercapacitive properties.

Zheng et. al. synthesized mesoporous Co_3O_4 nanoparticles with different textural parameters by using mesoporous silicas, KIT-6 and SBA-15, as templates and $Co(NO_3)_2 \cdot 6H_2O$ as precursor via an improved solid-liquid route [68] .He also studied the effects of calcination temperature and textural parameters on the electrochemical capacitive behaviors of Co_3O_4 samples. He found that the results of electrochemical tests showed the capacitance value of the sample decreases slightly with the increase of the calcination temperature and the maximum specific capacitance value of the samples can reach 370 F/g. He realized that the BET surface

area is the crucial factor for the capacitance value of the sample; and for mesoporous materials, large pore size and high ordered degree of mesopore are advantageous to the maintenance of the capacitance value at high discharging current.

2.7 Summary

In this chapter, the recent advances in metal oxide electrode materials for supercapacitors have been reviewed. It is unquestionable that metallic oxide materials play a key role in developing high-performance energy storage devices. The electrochemical performances of electrode materials are mainly depending on their morphology and size. Due to the high specific surface area of nanostructured materials, these materials can provide more active sites for electrochemical reactions, short diffusion pathways for both ions and electrons and effectively alleviate the volume change during charge-discharge process, leading to enhanced electrochemical performance. Nanostructured electrode materials with high capacity, good safety, long cycle life and good reliability will undoubtedly boost the performance of lithium ion batteries and supercapacitors and facilitate their extensive application. In this thesis, study is emphasizing on cobalt oxide electrode materials with improved electrochemical performance for supercapacitors applications.

CHAPTER 3

RESEARCH HYPOTHESIS AND APPROACH

3.1 Statement of hypothesis

As discussed in the literature review, structure, morphology, electrolyte etc. influences the electrochemical behavior of oxide electrodes. In this study, the effort is to change the morphology of Co_3O_4 to achieve high surface area and subsequently assessed its electrocapacitive performance. The change in morphology of Co_3O_4 is achieved via hydrolyzing agent, urea, in this study. The influence of morphology on the electrochemical performance of Co_3O_4 electrodes will be `assessed via galvanometric study. Several routes such as solvothermal [69], thermal decomposition [70], hydrothermal [71], spray pyrolysis [72], electrostatic spray deposition [73], sol-gel [74], precipitation [75], electrospinning [76], anodic oxidation of alloys [77], rheological phase reaction and pyrolysis [78], gel hydrothermal oxidation [79], electrodeposition technique [80] etc. are available for the synthesis of Co_3O_4 nanostructures. Out of these methods, we have adopted hydrothermal synthesis method for the preparation of Co_3O_4.

3.2 Hydrothermal method

Hydrothermal method is a synthesis method of single crystals from high temperature aqueous solution at high vapour pressure [81]. The crystal growth is performed in an apparatus consisting of a steel pressure vessel called an autoclave, in which a nutrient is supplied along with water. The crystal growth in hot solvent under high pressure depends on the solubility of the precursors. Hydrothermal method can create crystalline phases that are unstable at the melting point temperatures. The hydrothermal method can also grow materials that have a high vapour pressure near their melting points. This method is particularly suitable for the growth of many crystals with various morphologies and is widely used to prepare nanostructured materials.

Synthesis conditions can affect the morphology, composition and crystal structure of the materials. These include the temperature, the volume of the solvent, the concentration of the precursors and the use of a surfactant. The autoclave used in this study is made of stainless steel and the inside contains a polytetrafluoroethylene (PTFE) lined with 50 ml capacity, which is shown in **Fig. 3.1** (a and b). In this study, hydrothermal method was employed to synthesize Co_3O_4 nanostructure, which is presented in Chapter 4.

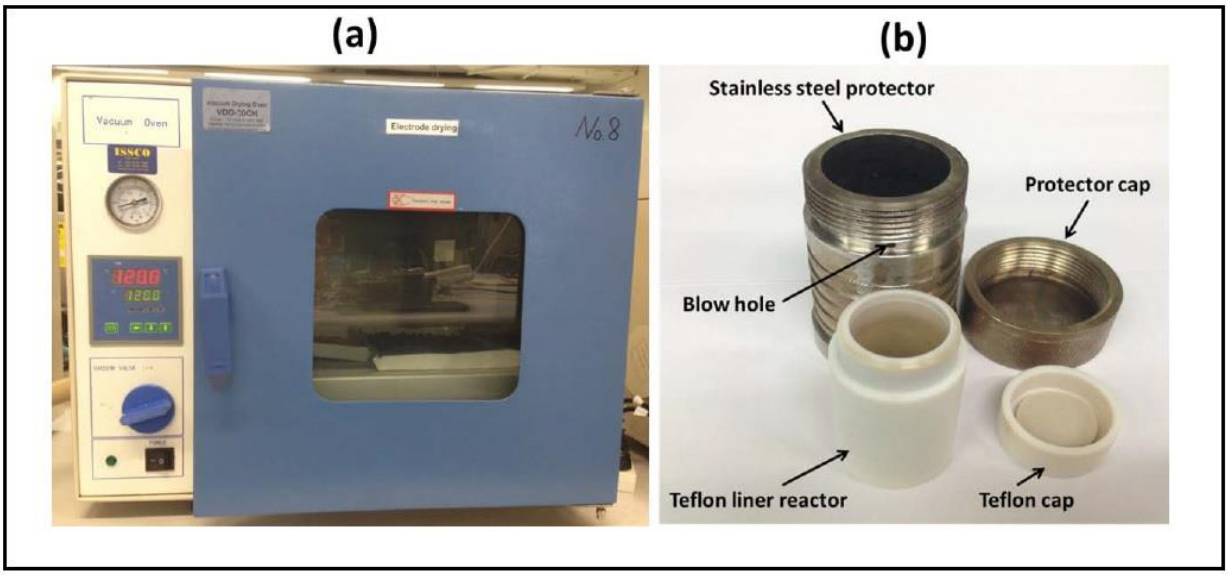

Fig.3.1. (a) Electric oven and (b) Autoclaves for hydrothermal synthesis [69].

3.3 Urea as hydrolysis Agent

Morphology plays a significant role in the electrochemical properties So It is much dependent on the adapted synthesis techniques. Particularly the use of oxidizer, complexing, and dispersing agent is essential in controlling the morphology of the particles [69]. Urea is chosen as a forced-hydrolysis agent in this study as it is water soluble in temperatures between 80 and 100 ° C, and gradually decomposed into NH_3 and CO_2 [82]. Further NH_3 reacts with water to produce NH_4^+ and OH^- as shown below;

$$CO(NH_2)_2 + H_2O \rightarrow 2\,NH_3 + CO_2\uparrow$$

$$NH_3 + H_2O \rightarrow NH_4^+ + OH^-$$

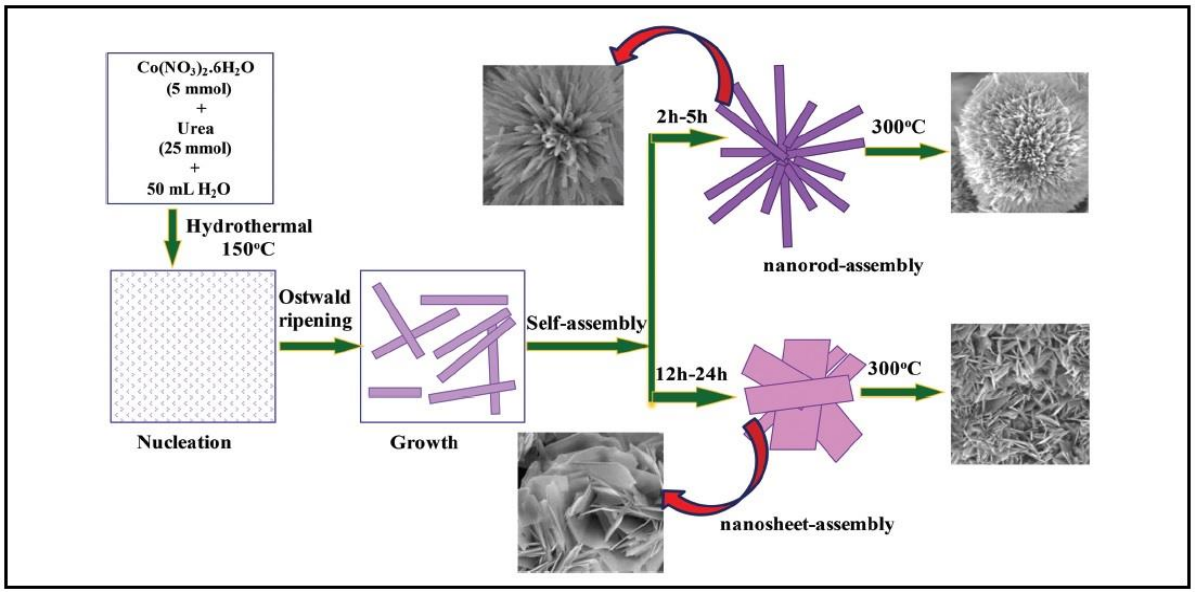

Fig.3.2. Schematic representation of the proposed formation mechanism for shaped Co_3O_4 [83].

According to schematic **Fig.3.2**, It is clear that urea plays an important role in the formation of structures along with hydrothermal time too. The formation of NH_3 and CO_2 from urea exists in the form of bubbles in aqueous solution [84,85]. These bubbles acts as soft templates. At the initial stage, the nanoparticles of hydrated cobalt hydroxy carbonate grow around the bubbles forming a hierarchical structure in which the particles are loosely packed. By Ostwald ripening, the particles grow along a certain crystallographic axis with the exposure of the plane forming different structures [74]. In the oxide crystal growth process, tiny crystalline nuclei are formed, and nanoparticles of this oxide gets precipitated by an increase in pH due to NH_4^+ ions generated from of NH_3 as a result of urea decomposition with increased temperature. The hydrolysis of urea leads to a rise in the pH due to increased release of NH_4^+ in the solution. The urea hydrolysis progresses slowly, and the basic solution undergoes supersaturation of the metal-hydroxide species [86,87]. Thus, the formation of metal-oxide occurs by a nucleation process with the preferred growth direction of the crystal. Furthermore, by the formation of gas molecules and an increase in the pressure in the hydrothermal system is expected to perturb

nanocrystalline growth and thereby may result in morphological changes. Under mild reaction conditions, hydrothermal time and temperature ~180 ˚C, this added factor may accelerate the reaction between the synthesis precursors and lead to anisotropic crystal growth and the crystallization of oxide.

3.4 Proposed Tasks

The purposed task is to synthesize of Co_3O_4 nanostructures with different urea concentration, study crystal structure, phase, morphology using SEM, XRD, Raman and FTIR, surface study using BET and electrochemical performance using potentiostat.

CHAPTER 4

EXPERIMENTAL

4.1 Sample preparation

Weighing advantages and disadvantages of the various synthesis route as discussed in the literature review section, a prudent choice was made in favor of hydrothermal technique to synthesis Co_3O_4. Samples were prepared via hydrothermal method using cobalt nitrate hexahydrate salt and urea, in which metal nitrates acted as an oxidizing reactant and urea is as a hydrolyzing agent (combustion fuel). This process is simple, safe, and rapid process where in main advantages are high homogeneity, high purity, time saving and ultrafine powders.

The hydrothermal process, in which the chemical reaction could take place under auto-generated pressure upon heating, is efficient to achieve the crystalline phase at relatively low temperatures. The hydrothermal process proceeds with aqueous and/or non-aqueous systems as the reaction medium and is environmentally friendly since the reactions are carried out in a closed system. The phase, particle size, and crystallinity can easily be controlled by hydrothermal conditions [88]. In particular, the particles prepared through hydrothermal synthesis are expected to have large surface area, smaller crystallite size, and higher stability than those obtained by other methods.

Chemicals required for the synthesis were purchased from Sigma Aldrich. Stoichiometric amount of Co $(NO_3)_2.6H_2O$ and different weight concentration (Molar Ratio /Mass Ratio=4, 2, 0.5, 0.3, 0.15) of urea (Co $(NH_2)_2$) were dissolved in a minimum amount of deionized water (35 ml) by stirring on a hotplate at 60 ˚C for 30 minutes. Then the entire solution was transferred to a 45 mL Teflon lined autoclave and maintained at 180 ˚C for 10 h and then cooled to room temperature naturally The precipitates were collected and washed with water and ethanol several

times by centrifugation and then dried at 80 ˚C for overnight. All of the as-synthesized intermediate products were calcined at 350 ˚C in air for 3.5 hrs.

The balanced chemical reaction for process is given as:

Hydrothermal reaction: $2Co(NO_3)_2 + 2CO(NH_2)_2 + 5H_2O \rightarrow Co_2(OH)_2CO_3\downarrow + 4NH_4NO_3 + CO_2\uparrow$

Heat-treatment: $3Co_2(OH)_2CO_3 + O_2 \rightarrow 2Co_3O_4 + 3H_2O\uparrow + 3CO_2\uparrow$

The detail amount of chemicals used for the synthesis of Co_3O_4 is summarized in the **Table 4.1.**

TABLE 4.1. DETAILS OF THE CHEMICALS USED FOR PREPARATION OF Co_3O_4

Sample	$Co(NO_3)_2.6H_2O$ (gm)	Urea (gm)
Co_3O_4-U2.99	3.626	2.993
Co_3O_4-U1.49	3.626	1.497
Co_3O_4-U0.37	3.626	0.374
Co_3O_4-U0.22	3.626	0.224
Co_3O_4-U0.11	3.626	0.112

4.2 Sample characterization

4.2.1 X-ray diffraction (XRD)

X-ray diffraction is a non-destructive analytical characterization technique to determine the crystal phase and structure. It generates an x-ray beam hitting a sample as a function of incident and scattered angle, polarization and wavelength or energy. A certain sample has a particular arrangement within the unit cell and this will lead to particular relative intensities of the recorded diffraction peaks upon x-ray hitting. Therefore, the unit cell size and geometry may be resolved from the angular positions of the x-ray diffraction results. The resultant diffraction lines with obvious peaks together are called an x-ray diffraction (XRD) pattern. Since the wavelength of x-ray is comparable to the size of atoms, they are suited for examining the structural arrangement of atoms and molecules in a wide range of materials. Each crystal has its unique characteristic x-ray diffraction pattern based on Bragg's law:

$$n\lambda = 2d \sin \theta \quad (5)$$

Where d is the interplanar spacing, θ is the Bragg angle, n is the order of reflection and λ is the wavelength of the x-rays irradiation.

In this research work, the basic use of XRD was to determine the actual phase of the material by comparing the obtained XRD pattern to the known standard diffraction lines in the International Centre for diffraction Data (ICDD) database. Samples were prepared by mounting the sample powder onto a low background glass disk. As the XRD test is non-destructive, the material can be reused for other tests. Structural characterization including phase purity, lattice parameter, crystalline size, lattice strain was performed on powder samples using x-ray diffractometer (D8 Advance Bruker Inc.) with Cu-Kα radiation (λ=1.54056 Å).

4.2.2 Scanning electron microscopy (SEM)

The scanning electron microscope (SEM) is a type of the electron microscope that images a sample by scanning it in a raster scan pattern with the excited beam of electrons. The electrons interact with the atoms that make up the sample producing signals that contain information about the sample's surface morphology. SEM is often used to obtain high magnification images to examine the details within nanostructured materials (around 1 nm in size). In this work, SEM was employed to characterize the morphology and surface structure of as pre-pared electrode materials. Its high-efficiency in-lens detector produces exceptional quality scanning electron images. The FESEM specimens can be prepared by spreading sample powder directly onto the carbon tape and then air-drying. All the measurements were carried out by using Phenom, SEM at 10 KV.

4.2.3 Brunauer-Emmett-Teller (BET) nitrogen adsorption-desorption isotherms

Brunauer-Emmett-Teller (BET) and Barrett-Joyner-Halenda (BJH) method are used to determine surface area, pore size and pore volume of the desired materials. BET analysis examines the external area and pore area of the materials to determine the total specific surface area those developers. BET analysis examines the external area and pore area of the materials to determine the total specific surface area in m^2/g by nitrogen multilayer adsorption isotherms. BJH analysis can also be employed to determine pore area and specific pore volume using nitrogen adsorption and desorption techniques to characterize pore size distribution of the sample. All the surface area measurements were carried out using Autosorb-1, (Quanta chrome, Boynton Beach, FL 33426, model no. AS1MP) using nitrogen as adsorb gas at 77 K.

4.2.4 Raman spectroscopy

Raman spectroscopy is a non-destructive spectroscopic technique used to study vibrational, rotational and other low-frequency modes in a molecular system. It relies on inelastic scattering, or Raman scattering of monochromatic light, such as laser. The laser light, in the Raman Microscope, is set to focus on the test sample. This allows interactions of the sample with its vibrations or excitations at a molecular level in the system, resulting in the energy of the laser photons being shifted up or down. The shift in energy gives information about the vibrational modes in the system. The resolution of the Raman spectra can be enhanced by accumulated scans with a longer exposed time. All the spectroscopy measurements were carried out using Thermo Scientific DXR Raman Microscope between 55 and 1000 cm^{-1} at 40 s exposure time.

4.2.5 Fourier transform infrared spectroscopy

Fourier Transform Infrared Spectroscopy (FTIR) is a technique used to obtain an infrared spectrum of absorption of a solid, liquid or gas sample. An FTIR spectrometer simultaneously

collects spectral data in a wide spectral range. This confers a significant advantage over a dispersive spectrometer that measures the intensity over a narrow range of wavelengths at time. Fourier transform infrared (FTIR) spectra were recorded on a Thermo Scientific (Nicolet iS10) between 450 and 900 cm^{-1}.

4.2.6 Electrode fabrication and cell assembly

4.2.6.1 Electrode fabrication

The Co_3O_4 electrodes were prepared by mixing 80 wt. % of the synthesized sample (Co_3O_4), 10 wt. % of acetylene black, and 10 wt. % of poly-vinylidene difluoride (PVDF). The three ingredients are mixed thoroughly in a mortar followed by the addition of a small amount of N-methyl pyrrolidinone (NMP) solution to form slurry. After mixing the components, the slurry was pasted onto nickel foam and pressed. The prepared electrode was dried at 60 ˚C under vacuum overnight. The electrochemical measurements were performed using a standard three-electrode system on a Versa STAT 4-500 electrochemical workstation (Princeton Applied Research, USA). The active material loading is around 1 mg.

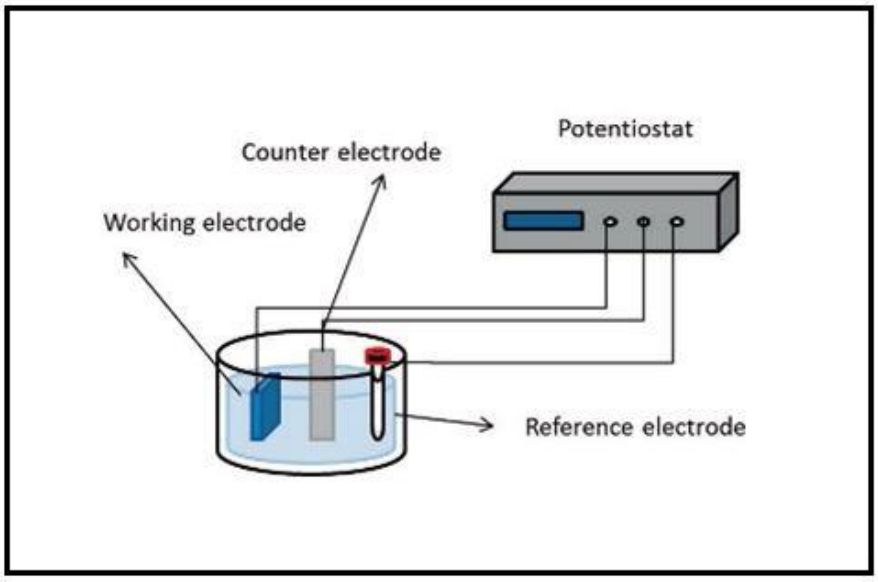

Fig.4.1. Schematic representation of the electrochemical cell [89].

4.2.6.2 Cell assembly

For supercapacitor test, beaker-type three-electrode cell was assembled with a working electrode facing a counter electrode (platinum foil) and reference electrode (saturated calomel electrode, SCE), which was placed close to working electrode. **Fig.4.1** shows the schematic representation of the electrochemical cell. In this study 3 M KOH was used as an electrolyte. Before electrochemical testing, the three-electrode cell was left for one or two hours so that the electrolyte solution can penetrate into the working electrode.

4.2.7 Electrochemical measurements

Electrochemistry is a branch of chemistry that studies chemical reactions that take place in a solution at the interface of an electron conductor and an ionic conductor, and which involve electron transfer between the electrode and the electrolyte or species in solution. In this study, the electrochemical properties were evaluated by cyclic voltammetry and galvanostatic charge-discharge, which are discussed below.

4.2.7.1 Cyclic voltammetry

Cyclic voltammetry (CV) is an important tool to study electrochemical reactions (oxidation and reduction) and the electrochemical reversibility. It is a type of potentiodynamic measurement that can be used to record a relationship of current vs. voltage. The measurement is taken when the potential at the working electrode is ramped linearly versus time (at a particular scan rate) to a set potential and reversed back to the original potential at the same scan rate.

For lithium ion batteries and supercapacitors, an ideal CV curve for a reversible reaction consists of two peaks opposite each other, as one process is anodic and the other is cathodic, and further confirm the energy storage mechanism involved. In this thesis, CV was conducted using a

standard three-electrode system on a Versa STAT 4-500 electrochemical workstation (Princeton Applied Research, USA) at different scan rates and voltage ranges at room temperature.

4.2.7.2 Galvanostatic charge-discharge

For three-electrode supercapacitors test system, the galvanostatic charge-discharge performance is examined by a chronopotentiometry technique on an electrochemistry workstation with an aqueous electrolyte.

CHAPTER 5

RESULT AND DISCUSSION

5.1 Structural study: x-ray diffraction

The x-ray diffraction (XRD) pattern of Co_3O_4 sample heated at 350°C for 3.5 hrs is shown in **Fig.5.1**. No characteristic peaks from other impurities are observed in the XRD pattern, indicating that the sample was highly pure. All the reflections can be indexed to the typical Co_3O_4 phase (space group $Fd\bar{3}m$ [227]), and corresponding to the standard crystallographic data depicted by International Centre for Diffraction Data (ICDD) card no. 02-0770. No secondary or impurity phases were detected, indicating high purity of the final products. The main peaks at 31.3°, 36.8°, 44.8°, 59.4° and 65.2° can be assigned to the (220), (311), (400), (511) and (440) reflections of Co_3O_4 respectively. The crystallite size of the Co_3O_4 is estimated by the Scherrer's formula [90], and the average calculated size is listed in **Table 5.1**. The average crystallite size of Co_3O_4 falls in the range of 14.80 nm to 54.53 nm. Furthermore, the sharp diffraction peaks indicate the crystallization of calcined Co_3O_4 nanostructures. It is also interesting to note the influence of urea content on lattice constant that is the lattice constant of samples increases with the decrease in the urea concentration.

TABLE 5.1. LATTICE PARAMETER AND CRYSTALLINE SIZE OF Co_3O_4 NANOSTRUCTURES

Sample	a (Å)	Crystallite size (nm)
Co_3O_4-U2.99	8.01	14.80
Co_3O_4-U1.49	8.20	15.02
Co_3O_4-U0.37	8.52	17.74
Co_3O_4-U0.22	8.91	24.06
Co_3O_4-U0.11	9.09	54.53

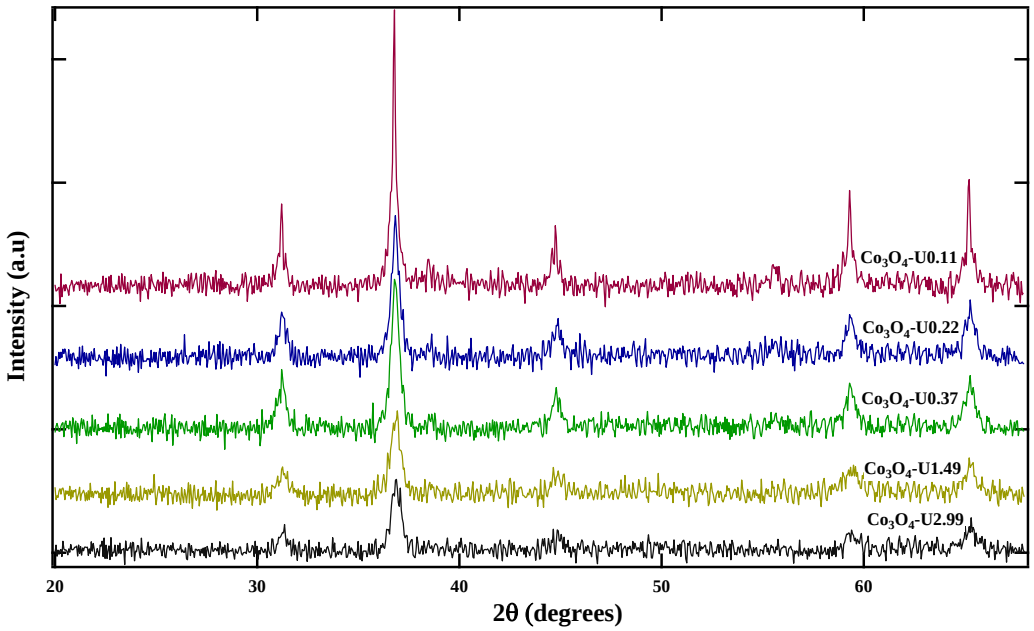

Fig. 5.1. XRD patterns of Co_3O_4 with different urea concentrations.

The decrease in urea content brings in lattice expansion of the unit cell. In addition, comparing full width half maxima (FWHM) of diffraction peaks, it is evident that the crystallinity of samples increases with the decrease in the urea concentration. Thus Co_3O_4-U0.11 is highly crystalline with crystal size ~ 54.53 nm as compared to Co_3O_4-U2.99 with crystal size ~ 14.80 nm.

5.2 Structural study: SEM

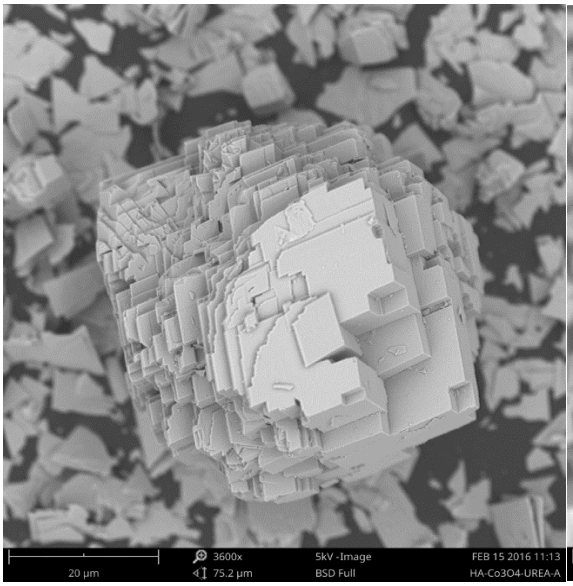

Fig.5.2 a) Co_3O_4-U2.99

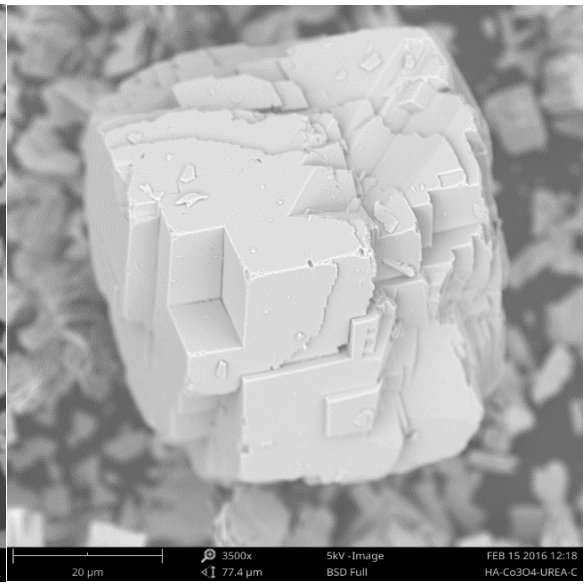

Fig.5.2 b) Co_3O_4-U1.49

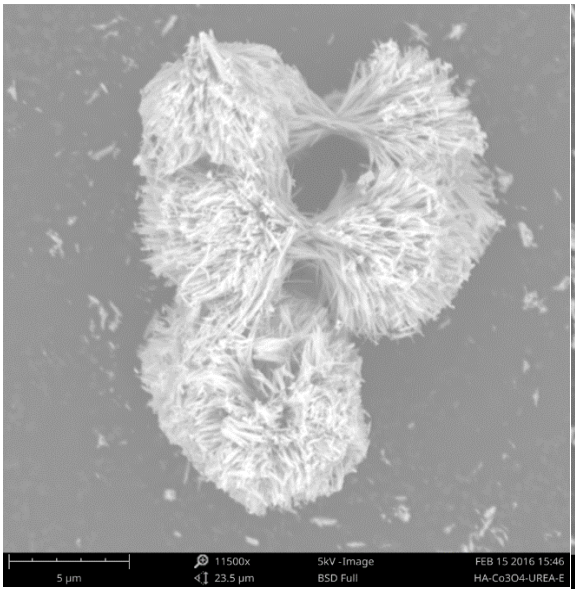

Fig. 5.2 c) Co_3O_4-U0.37

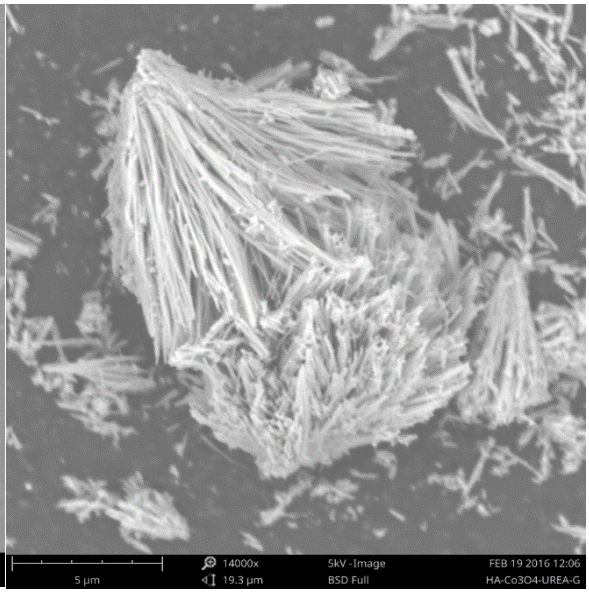

Fig. 5.4 d) Co_3O_4-U0.22

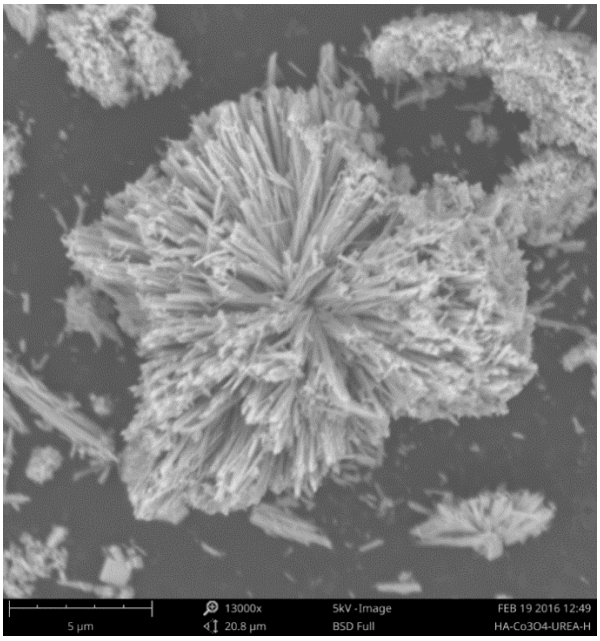

Fig. 5.2 e) Co_3O_4-U0.11

Fig.5.2. SEM images of the Co_3O_4 nanostructures with different urea concentrations (a) Co_3O_4-U2.99 **(b)** Co_3O_4-U1.49 **(c)** Co_3O_4-U0.37 **(d)** Co_3O_4-U0.22 **(e)** Co_3O_4-U0.11

As morphology plays a significant role in the electrochemical properties, morphological analysis of the obtained materials was conducted using SEM. Figure **5.2** shows the SEM images of Co_3O_4-U2.99, Co_3O_4-U1.49, Co_3O_4-U0.37, Co_3O_4-U0.22 and Co_3O_4-U0.11. Co_3O_4-U2.99 and Co_3O_4-U1.49 particles show plate like architecture while Co_3O_4-U0.37, Co_3O_4-U0.22 and Co_3O_4-U0.11 shows brush like morphology. It is interesting to note the change in morphology of Co_3O_4 with change in urea concentration. The morphology of Co_3O_4 samples from cubic plate like structure gradually went to brush like structure at low urea content. The decreased thickness of the architecture usually means higher surface area and thus, greater improvements in the performance of an electro-active material were expected. Usually, porosity of the electrode material provides large surface area and an easy access for the electrolyte, and thereby facilitates redox reactions during charge/discharge process. Therefore, porous microstructures of the current Co_3O_4 electrodes are very much desired for enhanced performance of supercapacitors. It

is to be noted that the morphology of Co_3O_4 is much dependent on the adapted synthesis techniques, which means the concentration of urea [91]. Particularly the use of oxidizer, complexing, and dispersing agent is essential in controlling the morphology of the particles [92].

5.3 Pore size distribution

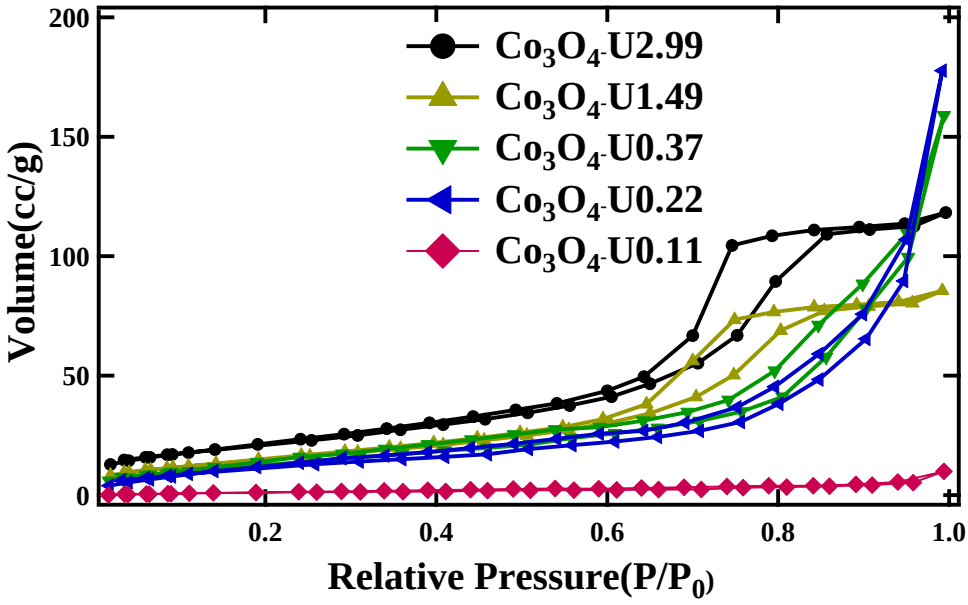

Fig. 5.3. The nitrogen adsorption/desorption isotherm of Co_3O_4 nanostructures.

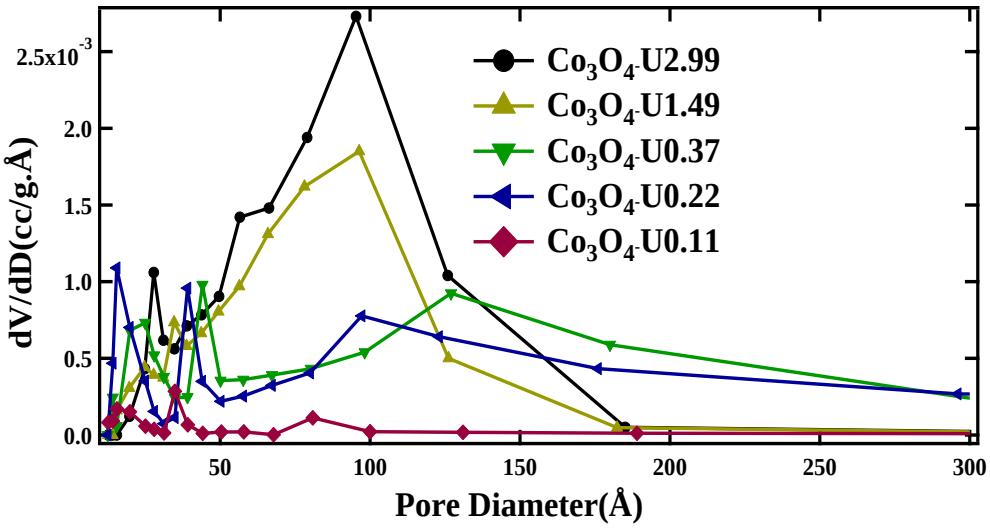

Fig. 5.4. The nitrogen adsorption/desorption pore size distribution curve of Co_3O_4.

The BET specific surface areas of Co_3O_4 was determined by N_2 adsorption-desorption isotherms at 77 K, and the corresponding pore size distributions were calculated by Barrette

Joynere Halenda (BJH) method, as displayed in **Fig.5.3**. The N_2 adsorption-desorption isotherm curves for all samples were measured at 77K between relative pressure $P/P_o \sim 0.029$ to 0.99. Important structural parameters are derived from the isotherms and tabulated in **Table 5.2**.

All samples display typical isotherm for mesoporous materials having hysteretic cycles at intermediate pressure, as represented by a type IV isotherms [93]. The measured surface area of cobaltite samples was 77.02 m^2/g for Co_3O_4-U2.99, 56.11 m^2/g for Co_3O_4-U1.49, 50.10 m^2/g for Co_3O_4-U0.37, 45.32 m^2/g for Co_3O_4-U0.22 and 4.72 m^2/g for Co_3O_4-U0.11 and were listed in **Table 5.2**. The width of hysteresis loops decreases in order of Co_3O_4-U2.99> Co_3O_4-U1.49> Co_3O_4-U0.37> Co_3O_4-U0.22> Co_3O_4-U0.11. On a side note, it is interesting to understand the adsorption-desorption behavior observed in Co_3O_4-U2.99. Co_3O_4-U2.99 exhibit "ink bottle" type hysteresis where the narrowing at the pore openings can deteriorate the access of the external gas phase to the pore interior on the desorption. A step in desorption isotherm is usually understood as a sign of interconnection of the pores [94,95]. The observed variation in isotherm hysteresis behavior of Co_3O_4-U2.99 is thus likely due to interconnected pore system while independent mesopores could be responsible for the hysteresis in Co_3O_4-U1.49, Co_3O_4-U0.37, Co_3O_4-U0.22 and Co_3O_4-U0.11 [96].The Fig **5.4** shows pore size distribution. From the curve, it can be observed that the largest number of pores is distributed at around 3 nm for Co_3O_4-U1.49, Co_3O_4-U0.37, Co_3O_4-U0.22 and Co_3O_4-U0.11 with the highest pore volume and should be more favorable for rapid ion transport within the electrode surface. Additionally, Co_3O_4-U2.99 also shows pore distribution at around 10 nm.

TABLE 5.2: SURFACE AREA PARAMETERS OF Co_3O_4 NANOSTRUCTURES.

Sample	BET Specific Surface area (m^2/g)	Total pore volume (cm^3/g)*	Average pore diameter (Å)
Co_3O_4-U2.99	77.02	$3.863*10^{-2}$	138.30
Co_3O_4-U1.49	56.11	$2.769*10^{-2}$	89.91
Co_3O_4-U0.37	50.10	$2.447*10^{-2}$	67.51
Co_3O_4-U0.22	45.32	$2.174*10^{-2}$	48.90
Co_3O_4-U0.11	4.72	$2.048*10^{-3}$	86.13

*****diameter less than 26.4 Å at $P/P_o = 0.3082$

5.4 Raman Study

Raman spectroscopy is a non-destructive approach to characterize nanostructures, in particular to determine ordered and disordered crystal structures of materials [97]. **Fig. 5.5** shows the Raman spectra of the Co_3O_4 nanostructures displayed in five bands in the range 100–1000 cm^{-1}. The signals located at approximately 187, 473, 515, 609, and 680 cm^{-1} correspond to the F_{2g}, E_g, F_{2g}, F_{2g}, and A_{1g} modes, respectively, of the crystalline Co_3O_4 phase in agreement with the literature values [98]. No vibrational modes due to impurities were observed. The band at 680 cm^{-1} is attributed to the characteristics of the octahedral sites (CoO_6), which is assigned to the A_{1g} species in the O_h^7 spectroscopic symmetry [99,100]. The Raman bands with medium intensity located at 473 and 515 cm^{-1} have the E_g and F_{2g} symmetry, respectively, whereas the weak band located at 609 cm^{-1} has the F_{2g} symmetry. The band at 187 cm^{-1} is attributed to the characteristics of the tetrahedral sites (CoO_4), which is attributed to the F_{2g} symmetry [79]. This result further confirms the formation of the Co_3O_4 nanostructures. The phonon symmetries of the Raman peaks are caused by the lattice vibrations of the spinel structure, in which Co^{2+} and Co^{3+} cations are situated at tetrahedral and octahedral sites in the cubic lattice [101].

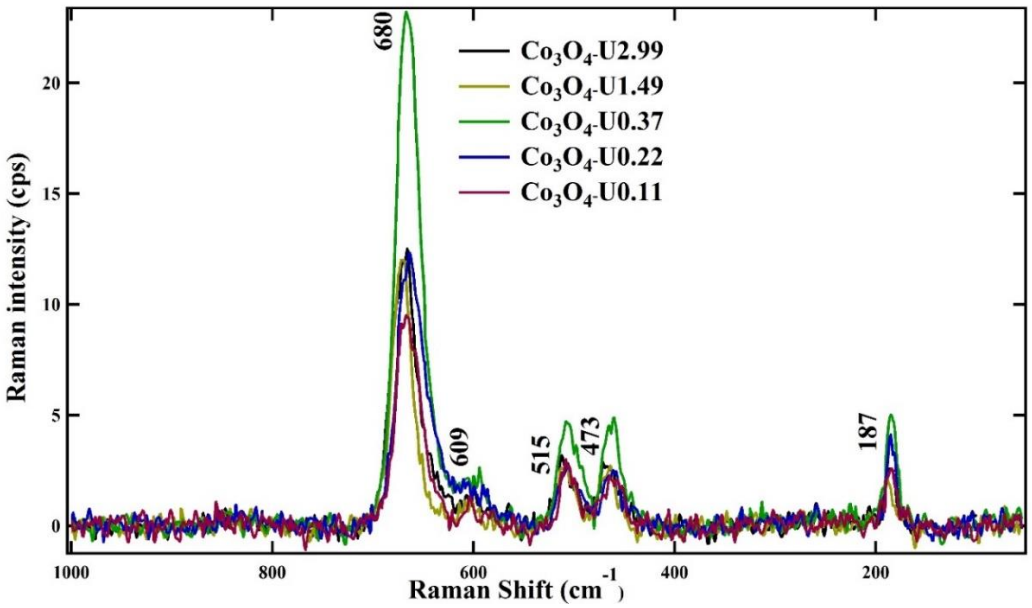

Fig. 5.5. Micro-Raman spectra of Co_3O_4 nanostructures.

5.5 FTIR study

Fig. 5.6 shows that the Fourier transform IR spectra for the synthesized Co_3O_4 nanostructure. The IR spectrum displays two distinct and sharp bands at 578.05 (ν_1) and 664.61 (ν_2) cm^{-1}, which originate from the stretching vibrations of the metal–oxygen bond [102,103,104]. The ν_1 band is characteristic of OCo3 vibrations (Co^{3+} in octahedral coordination), and the ν_2 band is attributable to $Co^{2+}Co^{3+}O_3$ (Co^{2+} in tetrahedral coordination) vibrations in the spinel lattice [105].The presence of these bands confirms the formation of phase-pure Co_3O_4 nanostructure.

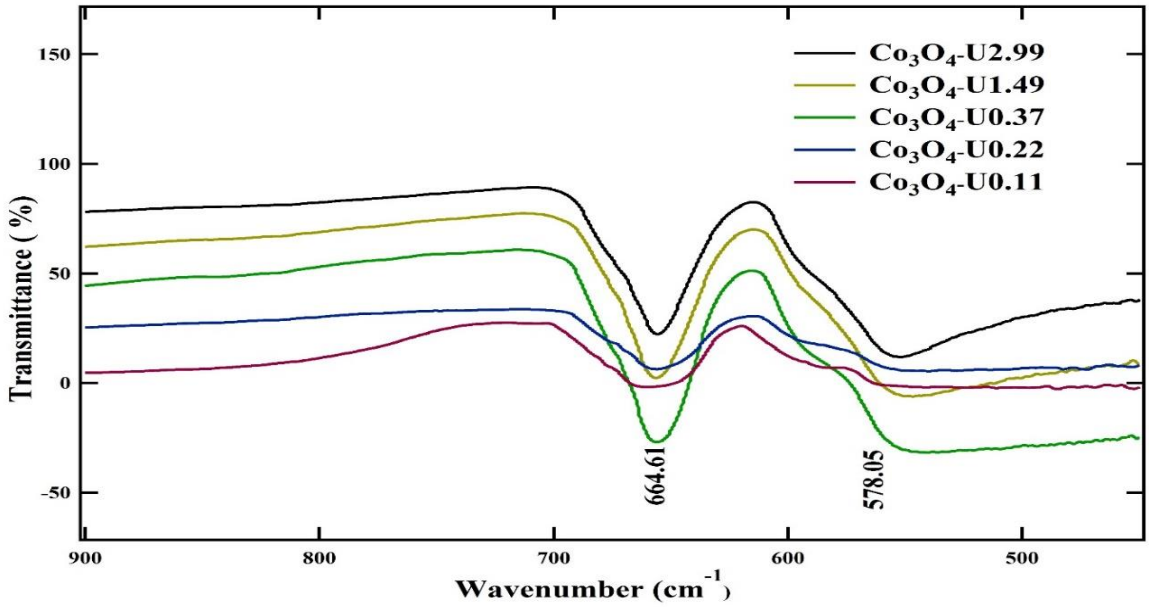

Fig. 5.6. FTIR Spectrum of Co_3O_4 nanostructures.

5.6 Electrochemical performance of Co_3O_4 nanostructures

The electrochemical performances of Co_3O_4 nanostructures as electrode materials for pseudocapacitors were evaluated by cyclic voltammetry measurement and galvanostatic charge/discharge.

Fig. 5.7 shows the cyclic voltammograms obtained at different scan rates (5–300 mV/s) in a voltage window of 0–0.6 V (vs. SCE). The capacitance characteristic of the Co_3O_4 nanostructures is that of typical pseudo-capacitance arising from reversible surface or near-surface Faradic reactions for charge storage. The detailed electrochemical process of the Co_3O_4 nano structures was illustrated by cyclic voltammograms (CVs). The redox reactions involved during the charge and discharge process, for example for Co_3O_4 can be described as follows [106]. Two typical redox couples are noticed in the CV curve. The first redox couple was attributed to the conversion between Co_3O_4 and CoOOH, expressed as follows:

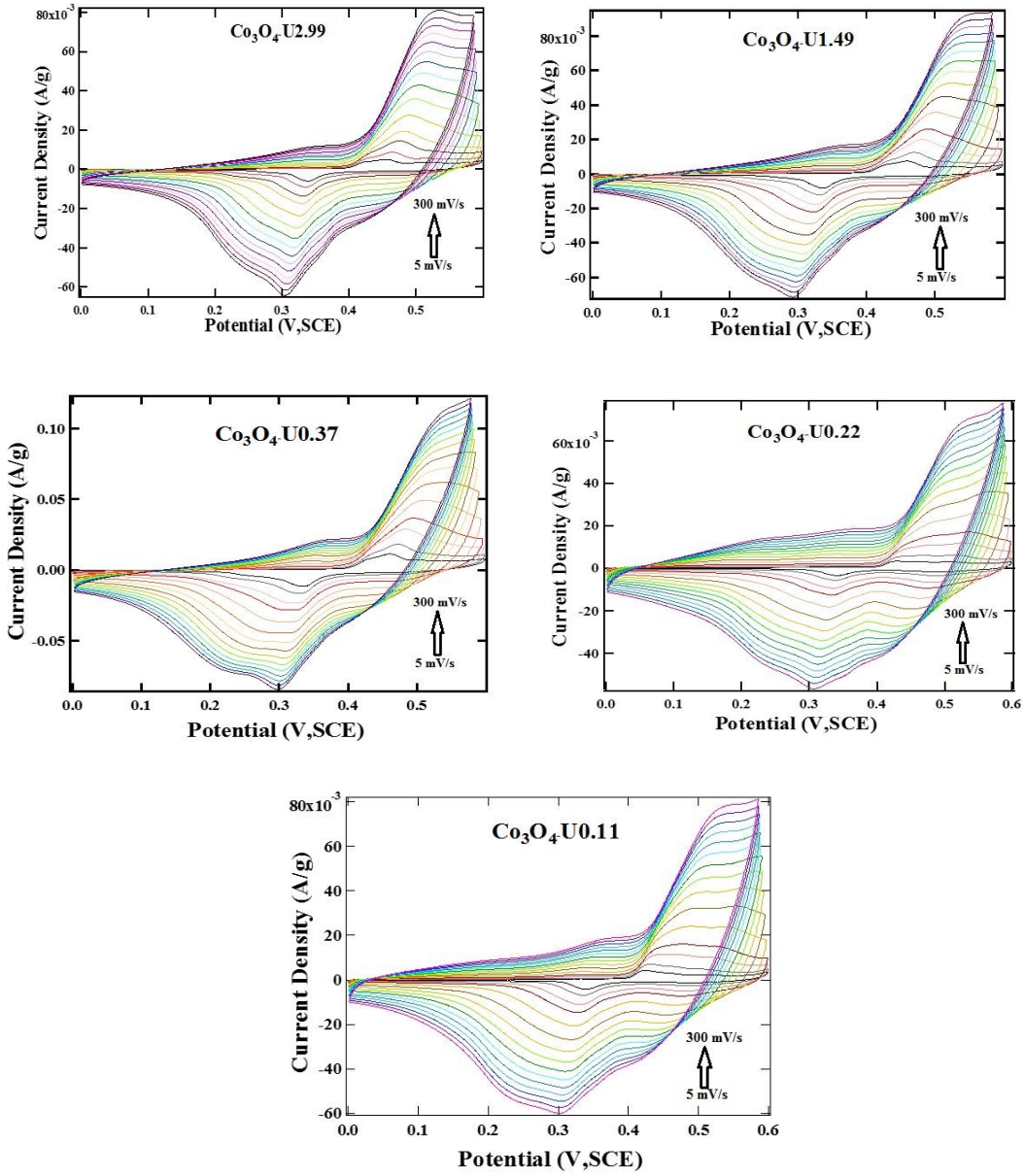

Fig. 5.7. CV curve of the Co_3O_4 nano structures on nickel foam substrate in the potential region of 0 – 0.6 V at different scanning rate from 5 mV/s to 300 mV/s.

$MO + OH^- \leftrightarrow 4MOOH + e^-$

$Co_3O_4 + OH^- + H_2O \leftrightarrow 3CoOOH + e^-$

The second redox couple corresponds to the reversible reaction between CoOOH and CoO_2, represented by the following reaction:

$CoOOH + OH^- \leftrightarrow CoO_2 + H_2O + e^-$

Non-rectangular form of CV curves is indicative of the pseudocapacitive characteristics of electrodes. A pair of reversible redox peaks can be observed within the potential range from 0 to 0.6 V. The anodic peak is due to the oxidation of Co_3O_4 to CoO_2 while the cathodic peak is for the reverse process. A small positive shift of the oxidation peak potential and a negative shift of the reduction peak potential have been observed with increased scan rate, which can be primarily attributed to the influence of the increasing electrochemical polarization as the scan rate scales up. Pairs of reversible redox curve indicating pseudocapacitance behavior of the material with redox peaks attributed M(II)/M(III) redox couples [107]. The shape and redox potentials of the CV curves are comparable to those reported for cobaltite [108],suggesting that the measured capacitance is mainly due to the redox mechanism. Furthermore, cathodic sweeps of CV curves are not completely symmetric to their corresponding anodic sweeps, which denotes some irreversibility. Asymmetric CV curve depicts the rate kinetics of the redox reactions were quasi reversible. Factors like polarization during faradaic redox reaction for pseudocapacitors and ohmic resistance due to electrolyte diffusion into the porous electrode kinetically limits the reversibility for the positive and negative sweeps [109]. It can be clearly observed that there is a pair of broad cathodic-anodic peaks, which becomes prominent at a higher scan rates.CV shape changes and shift in peak potential with increasing the scan rate indicate low polarization and high power characteristics of electrode material. At low scan rates, all the active specimen of the electrode material was fully utilized, whereas diffusion of ions to the innermost sites was hindered at high scan rates. Porous nature of the material felicitates rapid insertion/exertion of electron during redox reaction.

For diffusion control process the peak current density is related to the square root of the scan rate, $v^{1/2}$, via the following Randles-Sevcik [110,111] equation: $i_p = (2.687x10^5)\, v^{1/2}\, n^{3/2}\, D^{1/2}$

C. In this equation, n is the number of electrons appearing in half-reaction for the redox couple, v is the sweep rate, C, D is the concentration and the diffusion coefficient of the diffusing species. The slope and hence the diffusion coefficient D per unit area, for Co_3O_4-U0.37 is highest (~ D/A=0.007566 s^{-1}) and lowest for Co_3O_4-U2.99 (D/A ~ 0.005126 s^{-1}). As evident from **Fig.5.8**, the linear behavior of the curve for all sample shows presence of diffusion controlled process in all Co_3O_4 structures. In addition, higher peak current density for Co_3O_4-U0.37 signifies higher electrochemical reaction activity.

The average specific capacitance of the four samples were calculated from the CV curves based on the following equation [22]:

$$C = \frac{1}{mu(V_2 - V_1)} \int_{V_1}^{V_2} I(V)dV \qquad (6)$$

Where I (A) is the current, m (g) is the mass of the active material, u (V/s) is the scan rate, V_1 and V_2 (V) are the start and end voltage of the CV scan.

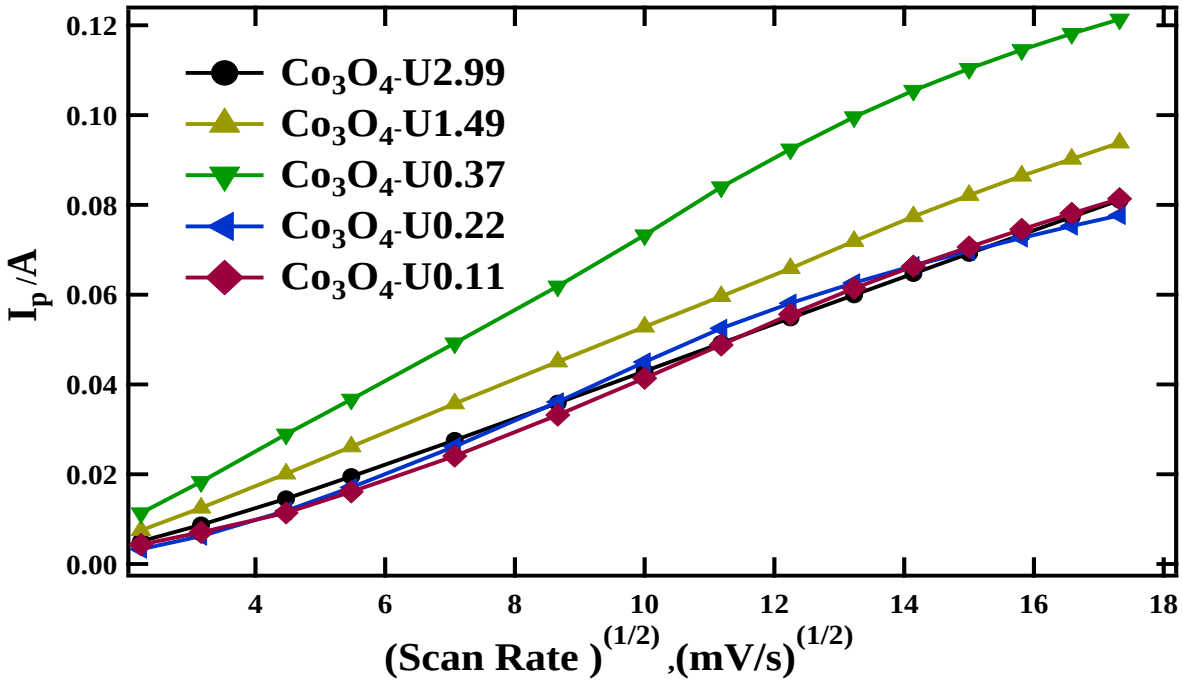

Fig. 5.8. Peak current vs. square root of scan rate of Co_3O_4 nano structures.

The average specific capacitances of all the Co_3O_4 samples calculated at various scan rates were presented in **Fig. 5.9**. The specific capacitance of Co_3O_4 nanostructures was calculated as 479, 510, 764,213 and 240 F/g at the scan rate of 5 mV/s for Co_3O_4-U2.99, Co_3O_4-U1.49, Co_3O_4-U0.37, Co_3O_4-U0.22 and Co_3O_4-U0.11, respectively. Among all Co_3O_4 nanostructures, Co_3O_4-U0.37 exhibited the highest capacitance for all scan rates with maximum value of 764 F/g at 5 mV/s scan rate. While other Co_3O_4 with different urea concentration display considerably lower value of specific capacitance between 100-510 F/g. These high values of specific capacitance can suggest a relatively high electrochemical utilization and high surface area of the synthesized nanostructures of Co_3O_4. It is worth noting that the porous morphology of the Co_3O_4 nanostructures caused better electrolyte penetration in the plates and so exhibited high contribution to the redox reactions [112]. From the CV curves at various scan rates, it can be noticed that the peak current increases with increasing the scan rate and difference in the cathodic and anodic peak potential expands gradually, indicating diffusion controlled reaction kinetics [113].

TABLE 5.3: SPECIFIC CAPACITANCES OF CO_3O_4 NANOSTRUCTURES AT DIFFERENT SCAN RATES.

Scan Rate (mV/s)	Specific Capacitance (F/g)				
	Co_3O_4 -U2.99	Co_3O_4 -U1.49	Co_3O_4 -U0.37	Co_3O_4 -U0.22	Co_3O_4 -U0.11
5	478.98	510.43	763.37	212.60	240.18
10	409.71	434.18	622.60	204.18	224.41
20	346.09	369.94	519.41	196.81	215.56
30	316.13	338.15	456.52	189.72	210.75
50	283.93	302.29	395.03	177.09	200.97
75	259.75	270.16	348.49	163.61	188.82
100	242.56	247.03	314.49	152.01	177.69
125	227.79	228.91	287.73	142.18	167.74
150	216.26	213.34	265.57	132.74	158.80
175	205.49	200.00	246.66	125.66	150.92
200	196.02	188.78	230.40	119.30	143.89
225	187.35	178.63	216.30	113.66	137.56
250	179.49	169.60	203.98	108.61	131.81
275	172.19	160.86	193.06	104.05	126.56
300	165.41	154.12	183.25	99.86	121.80

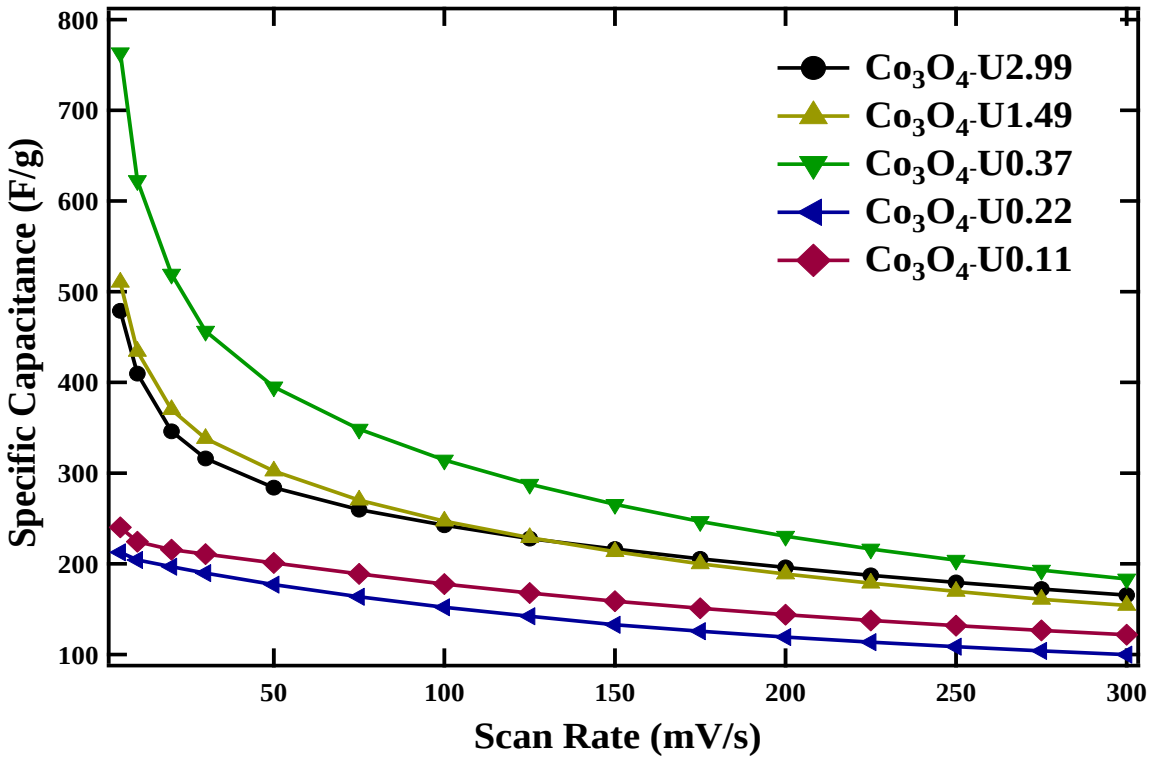

Fig. 5.9. Specific Capacitance vs Scan rate of Co_3O_4 nanostructures.

The rate capability and specific capacitance of the Co_3O_4 electrodes were performed using charge/discharge measurements. The charge storage capacity from the galvanostatic charge-discharge measurements was calculated using the following equation [114]:

$$C_{sp} = \frac{I\Delta t}{\Delta V m} \quad (7)$$

where, I is the discharge current (A), Δt is the discharge time (s), ΔV is the potential window (V),and m is the mass (g) of the active material.

The calculated specific capacitance as a function of current density is shown in **Table 5.3**. The specific capacitance of Co_3O_4-U2.99 is calculated to be 262.58, 234.28, 218.59, 205.54, 185.31, 170.18 and 156 F/g at current densities of 0.5,1,1.5,2,3,4,5 A/g with a capacity retention rate (as compared to 0.5 A/g) is 40.58 % at current density of 5A/g **(Fig.5.10).** The specific capacitance of Co_3O_4 -U1.49 is calculated to be 272.86,245.86,230.76,217.61,192.40,176.26, and 170.36 F/g at current densities of 0.5,1,1.5,2,3,4,5 A/g with a capacity retention rate (as compared to 0.5 A/g) is 37.57 % at current density of 5A/g. The specific capacitance of Co_3O_4-U0.37 is calculated to be 469.80, 416.90, 382.44,354.07, 307.13,278.39 and 256.21 F/g at current densities of 0.5,1,1.5,2,3,4,5 A/g with a capacity retention rate (as compared to 0.5 A/g) is 45.47 % at current density of 5A/g. The specific capacitance of Co_3O_4 -U0.22 is calculated to be 96.31, 95.23, 93.60, 92.21, 91.50, 88.11and 85.50 F/g at current densities of 0.5,1,1.5,2,3,4,5 A/g with a capacity retention rate (as compared to 0.5A/g) is 11.23 % at current density of 5A/g. The specific capacitance of Co_3O_4-U0.11 is calculated to be 107.98, 106.29, 105.40, 104.97, 103.96, 101.87 and 100.07F/g at current densities of 0.5,1,1.5,2,3,4,5 A/g with a capacity retention rate (as compared to 1 A/g) is 7.32 % at current density of 5A/g. When the current density increased from 0.5 A/g to 5 A/g the specific capacitances were noted to decrease. This was due to the presence of inner active sites that were incapable to take part complete redox

transitions at high current densities. This suggests that the some areas of the electrode surfaces were unreachable at high current densities. As seen, Co_3O_4 -U0.37 exhibits excellent 469.80 F/g capacitance while other Co_3O_4 show specific capacitance in the range of 85-272 F/g at all the current densities evaluated and show a good rate capability. The good electrochemical performance of Co_3O_4-U0.37 among all Co_3O_4 studied herein may be attributed to short diffusion length for the electrolyte ions through porous structure which allows enough electrolyte ions to rapidly contact the large surfaces of the electroactive and conducting Co_3O_4 nanoparticles. This ensure rapid and sufficient Faradaic reactions at high current densities for energy storage [115].**Table 5.4** compares the capacitance of the capacitance for the Co_3O_4 electrode material with other reported Co_3O_4 materials based electrodes in previous literatures.

TABLE 5.4: COMPARISON OF THE CAPACITANCE FOR THE Co_3O_4 ELECTRODE MATERIAL WITH OTHER REPORTED Co_3O_4 MATERIALS BASED ELECTRODES IN PREVIOUS LITERATURES.

Electrode Materials	Specific Capacitance	Rate Capability	Reference
Co_3O_4-U0.37	469.8 F/g at 0.5 A/g	45.7 % retention from 0.5 to 5 A/g	This work
Co_3O_4 nanoparticles	286 F/g at 4 A/g	73.5 % retention from 0.5 to 5 A/g	116
Co_3O_4 film	325 F/g at 2 A/g	24 % retention from 2 to 40 A/g	117
Co_3O_4 nanowire	295 F/g at 2 A/g	16.27 % retention from 2 to 40 A/g	118
Dendrite-like Co_3O_4 nanostructures	207 F/g at 0.5 A/g	36.1% retention from 0.5 to 6 A/g	119
Mesoporous Co_3O_4 nanocubes	350 F/g at 0.2 A/g	45.7 % retention from 0.2 to 2 A/g	120
Hollow Co_3O_4 boxes	278 F/g at 0.5 A/g	63.3 % retention from 0.5 to 5 A/g	121
Co_3O_4/Carbon composites	400 F/g at 0.5 A/g	37.5 % retention from 0.5 to 5 A/g	122
Co_3O_4/RGO composites	518. F/g at 0.5 A/g	47.6 % retention from 0.5 to 10 A/g	123
Co_3O_4 nanowire@MnO2 ultrathin nanosheets	480 F/g at 2.67 A/g	55.6 % retention from 2.67 to 29.8 A/g	124

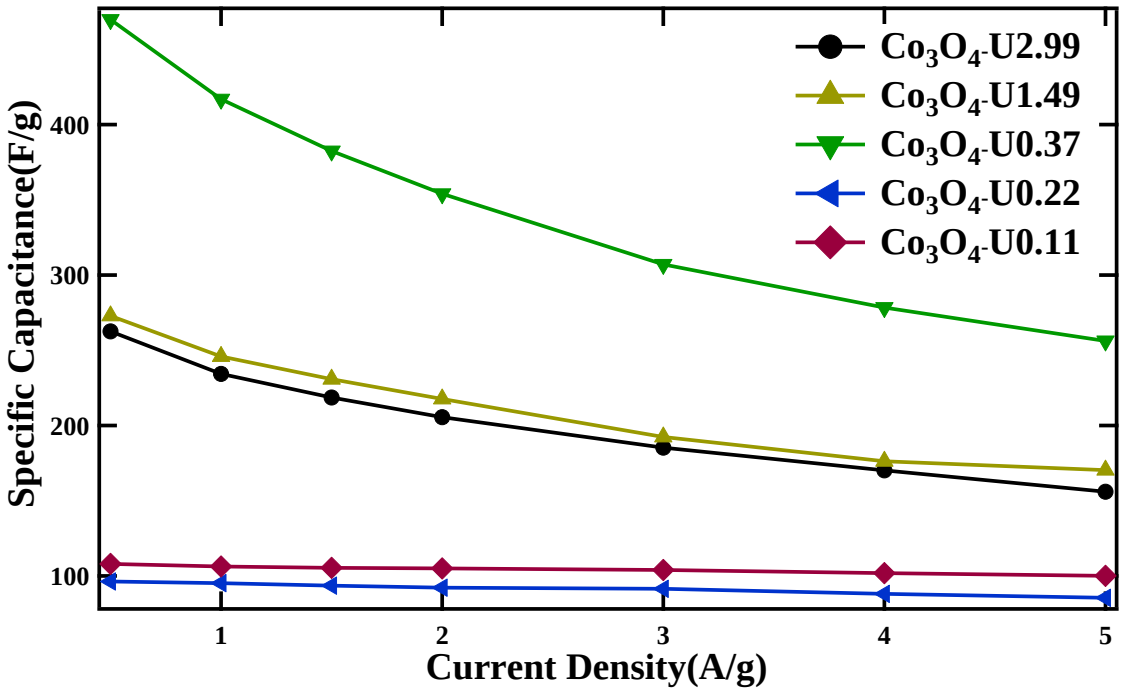

Fig. 5.10. Specific capacitance vs. current density of Co_3O_4 nanostructures.

TABLE 5.5: THE SPECIFIC CAPACITANCE OF THE CO_3O_4 AT DIFFERENT CURRENT DENSITIES.

Current Density (A/g)	Specific Capacitance (F/g)				
	Co_3O_4-U2.99	Co_3O_4-U1.49	Co_3O_4-U0.37	Co_3O_4-U0.22	Co_3O_4-U0.11
0.5	262.58	272.86	469.80	96.31	107.98
1	234.28	245.86	416.90	95.23	106.29
1.5	218.59	230.76	382.44	93.60	105.40
2	205.54	217.61	354.07	92.21	104.97
3	185.31	192.40	307.13	91.50	103.96
4	170.18	176.26	278.39	88.11	101.87
5	156.00	170.36	256.21	85.50	100.07

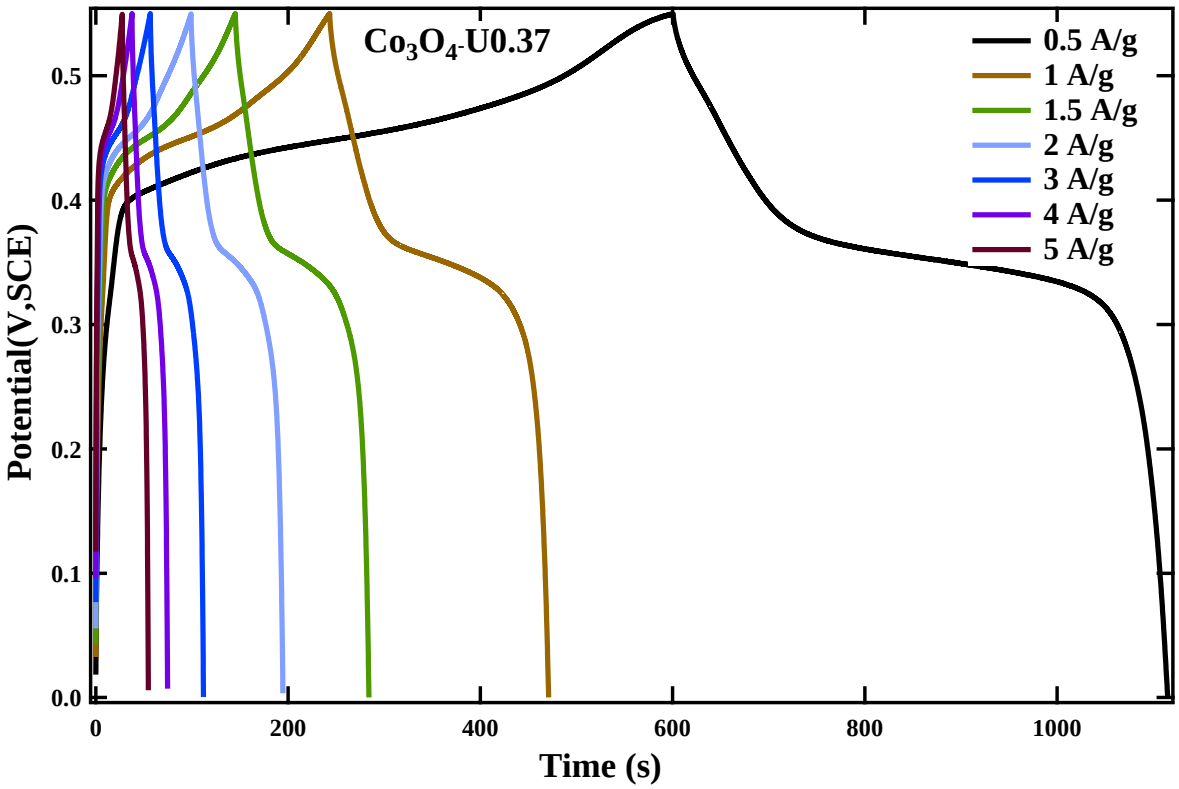

Fig. 5.11. Galvanic discharge characteristics of Co_3O_4-U0.37 nano structures at various discharge currents

To further, characterize the electrochemical performance, galvanostatic charge-discharge measurements were done. The galvanic charge/discharge cycles in **Fig. 5.11** tested at different current density 0.5, 1, 1.5, 2, 3, 4 and 5 A/g showed efficiency of Co_3O_4-U0.37 nanostructures, which indicates excellent reversibility of the electrodes during charge–discharge process and this could be attributed to the porosity and nanostructures of the active material as they provide large surface area with reduced charge and mass diffusion distances along with easy accessibility to the electrolyte [97]. The drop in potential during the discharge process can be attributed to the internal resistance of the electrode. A potential plateau was observed in charge-discharge curves, suggesting high electrochemical reversibility and fast reaction kinetics of Co_3O_4-U0.37 electrode indicating typical pseudocapacitance behavior of the electrode. This could be due to charge transfer reaction or electrochemical adsorption/desorption process at the electrode/electrolyte

interface. As seen, the specific capacitance of the electrode decreases with increasing current for all electrolytes. The decrease in the specific capacitance with the increasing discharge current could be due to increase in potential drop and insufficient faradic redox reaction at higher currents [125].

For potential applications, supercapacitors are rated in terms of their power density and energy density. Power density and energy density demonstrate the operational characteristics of supercapacitors. The Ragone plot is plotted to compare the energy and power density of Co_3O_4 as shown in **Fig. 5.12**. The measured energy and power density for all Co_3O_4 nanostructures is listed in **Table 5**. The energy densities (E) and power densities (P) of the electrochemical cells are calculated using the following equations: $E=(1/2)\ CV^2$ and $P=E/t$ where C is the specific capacitance that depends on the mass of the electrodes, V is the operating voltage of the cell and "t" is the discharge time in seconds as obtained from **Fig. 5.11.**

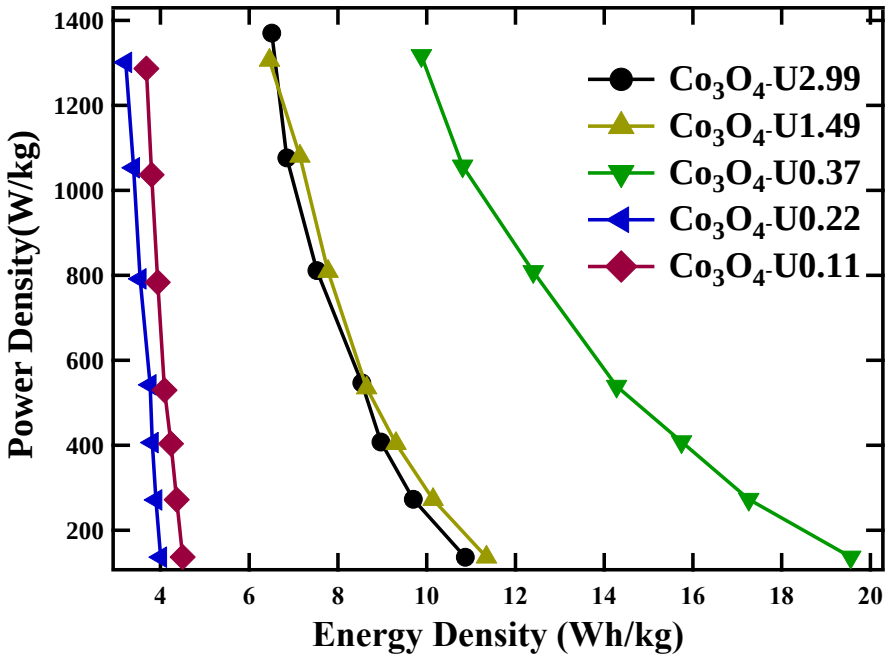

Figure 5.12. Ragone plot of Co_3O_4 nanostructures.

Table 5.6: SPECIFIC POWER DENSITY AND ENERGY OF AS SYNTHESIZED Co_3O_4 NANOSTRUCTURES AT DIFFERENT CURRENT DENSITIES OBTAINED FROM CHARGE-DISCHARGE CHARACTERISTIC CURVES.

Co_3O_4-U2.99		**Co_3O_4-U1.49**		**Co_3O_4-U0.37**		**Co_3O_4-U0.22**		**Co_3O_4-U0.11**	
ED	**PD**	**ED**	**PD**	**ED**	**PD**	**ED**	**PD**	**ED**	**PD**
10.87	136.48	11.35	136.79	19.56	136.87	4.00	136.79	4.50	136.94
9.70	272.97	10.14	272.51	17.26	272.97	3.90	271.43	4.37	271.90
8.97	407.61	9.31	404.16	15.74	408.30	3.81	406.23	4.24	403.47
8.54	546.86	8.65	534.90	14.28	538.88	3.77	542.26	4.09	529.68
7.53	811.08	7.78	809.24	12.40	808.78	3.54	791.76	3.94	783.48
6.85	1076.54	7.14	1080.22	10.81	1057.52	3.39	1053.23	3.80	1036.67
6.51	1370.21	6.46	1306.09	9.88	1317.30	3.22	1301.20	3.68	1286.63

ED=Energy Density (Wh/kg), PD=Power density (W/kg)

In terms of energy density performance, Co_3O_4 nanostructures are grouped into three regions. Co_3O_4-U0.11 and Co_3O_4-U0.22 with energy density around 4 Wh/kg, Co_3O_4-U1.49 and Co_3O_4-U2.99 with energy density around 11 Wh/kg and Co_3O_4-U0.37 with energy density 19.56 Wh/kg for different power density values. As known, the most important point for high performance supercapacitors is to obtain a high energy density and meanwhile providing an outstanding power density. The results showed that all Co_3O_4 nanostructures have performed well in terms of power density and Co_3O_4-U0.37 performed superior and high energy density performance as compare to other Co_3O_4 nanostructures.

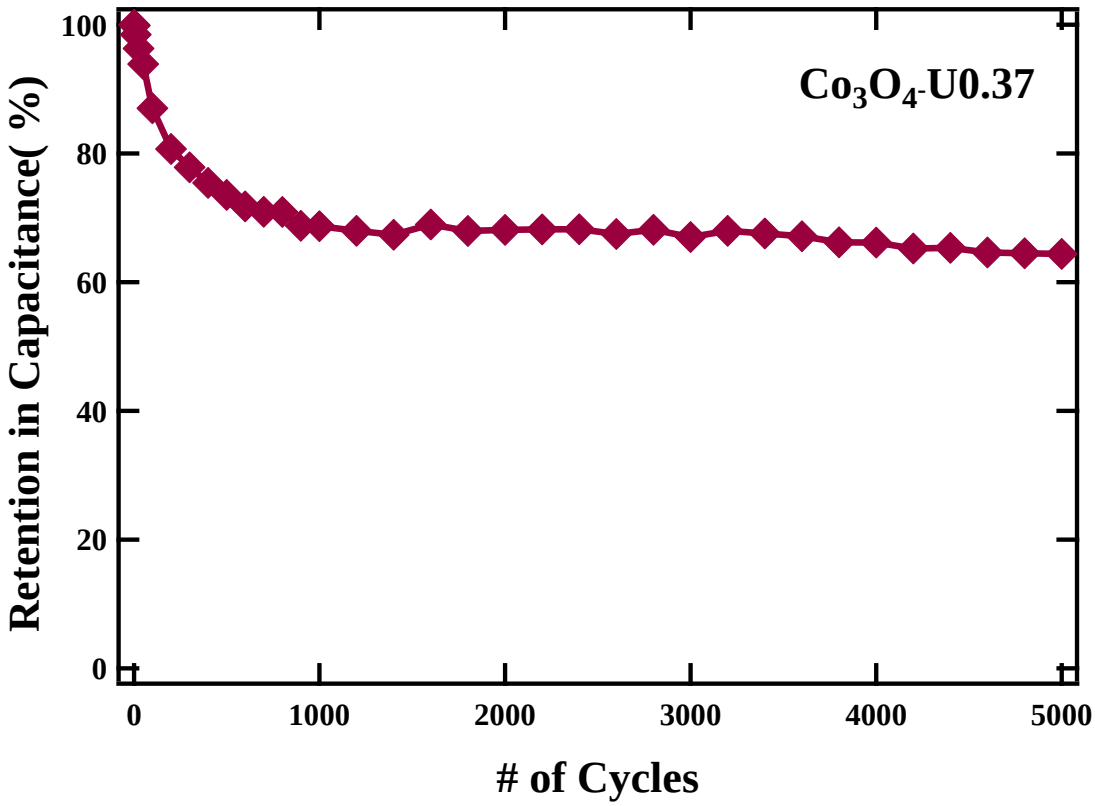

Fig. 5.13. Percentage change in specific capacitance vs. number of cycle for Co_3O_4-U0.37

The cyclic performance of any electroactive material is a significant parameter to be studied for its practical applications. The cyclic performance of Co_3O_4-U0.37 nanostructure was carried out at a current density of 0.5 A/g and was shown in **Fig. 5.13**. The specific capacitance of the electrode gradually decreased at higher cycle numbers to 64% of the initial capacitance value after 5000 cycles. The cyclic performance data clearly highlights the capability of the Co_3O_4-U0.37 nanostructure electrode meets the requirement of both long cycling performance and good rate capability, parameters that are important for the practical energy storage devices.

CHAPTER 6

CONCLUSION

Co_3O_4 electrode materials prepared by different urea concentration were successfully synthesized via simple hydrothermal process with calcination at 350 °C. The optimum specific capacitance was observed for Co_3O_4-U0.37. By comparing the electrocapacitive performance of Co_3O_4, it can be concluded that brush like open structures of Co_3O_4 is more discrete architecture for supercapacitors applications. The power and energy density clearly show that high power density can be retained at high energy density values.

It is shown that, the nanostructure affects the electrocapacitive behavior of electrodes. The study suggests a guide for optimizing the electrocapacitive behavior of electrode via alteration of nanoarchitecture of electrode. The electrochemical stability, excellent capacitive performance, and the easiness of the preparation method suggest this unique material system is promising for future high performance energy storage applications.

In conclusion, architecture of Co_3O_4 nanostructures was successfully altered using urea as a hydrolyzing agent. It is observed that low urea concentration leads to Co_3O_4 nanostructures with high electrocapacitive performance.

Future Work:

A further work is necessary to understand the electrocapacitive property of Co_3O_4.

a) A theoretical work is needed to understand the dependence of band gap on unit cell and lattice parameter. This will help to identify best possible lattice parameter leading to the high conductivity of Co_3O_4 and hence electrocapacitive performance.

b) Influence of various electrolyte (e.g. KOH, LiOH, NaOH) on the electrocapacitive performance of Co_3O_4 is to be assessed.

REFERENCES

[1] Fletcher, Seth. Bottled lightning: superbatteries, electric cars, and the new lithium economy, Macmillan, (2011).

[2] LaCommare, Kristina Hamachi, and Joseph H. Eto. "Understanding the cost of power interruptions to US electricity consumers." Lawrence Berkeley National Laboratory (2004).

[3] Whittingham, M. Stanley. "Materials challenges facing electrical energy storage." MRS Bulletin 33.04 (2008): 411-419.

[4] Holm, S. R., et al. "A comparison of energy storage technologies as energy buffer in renewable energy sources with respect to power capability." Proc. IEEE Young Researchers Symp. Electrical Power Engineering, Leuven, Belgium. 2002.

[5] Von Jouanne, Annette, Prasad N. Enjeti, and Basudeb Banerjee. "Assessment of ride-through alternatives for adjustable-speed drives."Industry Applications, IEEE Transactions on 35.4 (1999): 908-916.

[6] Wagner, Leonard. "Overview of energy storage methods." Analyst (2007).

[7] Simon, Patrice, and Yury Gogotsi. "Materials for electrochemical capacitors Nature materials 7.11 (2008): 845-854.

[8] Li, Peiwen. "Energy storage is the core of renewable technologies." IEEE Nanotechnology Magazine 4.2 (2008): 13-18.

[9] Conway, B. E., and W. G. Pell. "Double-layer and pseudocapacitance types of electrochemical capacitors and their applications to the development of hybrid devices." Journal of Solid State Electrochemistry 7.9 (2003): 637-644.

[10] Energy Storage Technologies: A Comparison" published by CAP-XX Ltd. Retrieved on November 7th, 2007 from http://www.cap-xx.com/resources/reviews/strge_cmprsn.htm

[11] What is SMES?" published by Ecole Polytechnique Fédérale de Lausanne. Retrieved on November 16th, 2007 from http://lanoswww.epfl.ch/studinfo/courses/cours_supra/smes/whatsmes.htm

[12] O'Neal, Audrey Pool. "The Effect of Particle Size and Processing on the Properties of a

Barium Titanate Polymer Composite." (2014).

[13] Miret, Santiago. "Storage Wars: Batteries vs. Supercapacitors." Berkeley Energy and Resources Collaborative, November 10 (2013).

[14] Buchmann, Isidor. "Battery university." When was the battery invented (2013).

[15] Winter, Martin, and Ralph J. Brodd. "What are batteries, fuel cells, and supercapacitors?" Chemical reviews 104.10 (2004): 4245-4270.

[16] Kötz, R., and M. Carlen. "Principles and applications of electrochemical capacitors." Electrochimica Acta 45.15 (2000): 2483-2498.

[17] Miller, John R., and Patrice Simon. "Electrochemical capacitors for energy management." Science Magazine 321.5889 (2008): 651-652.

[18] Burke, Andrew. "Ultracapacitors: why, how, and where is the technology."Journal of power sources 91.1 (2000): 37-50.

[19] Hadjipaschalis, Ioannis, Andreas Poullikkas, and Venizelos Efthimiou. "Overview of current and future energy storage technologies for electric power applications." Renewable and sustainable energy reviews 13.6 (2009): 1513-1522.

[20] Boyea, J. M., et al. "Carbon nanotube-based supercapacitors: technologies and markets." Nanotech. L. & Bus. 4 (2007): 19.

[21] Halper, Marin S., and James C. Ellenbogen. "Supercapacitors: A brief overview." The MITRE Corporation, McLean, Virginia, USA (2006): 1-34.

[22] Conway, B. E. "Electrochemical supercapacitor." Scientific Fundamentals and Technological Applications (1999).

[23] Conway, B. E., V. Birss, and J. Wojtowicz. "The role and utilization of pseudocapacitance for energy storage by supercapacitors." Journal of Power Sources 66.1 (1997): 1-14.

[24] Mastragostino, Marina, Catia Arbizzani, and Francesca Soavi. "Polymer-based supercapacitors." Journal of power sources 97 (2001): 812-815.

[25] Kim, Il-Hwan, and Kwang-Bum Kim. "Ruthenium oxide thin film electrodes for

supercapacitors." Electrochemical and Solid-State Letters 4.5 (2001): A62-A64.

[26] Zheng, J. P., and T. R. Jow. "A new charge storage mechanism for electrochemical capacitors." Journal of The Electrochemical Society 142.1 (1995): L6-L8.

[27] Zheng, J. P., P. J. Cygan, and T. R. Jow. "Hydrous ruthenium oxide as an electrode material for electrochemical capacitors." Journal of the Electrochemical Society 142.8 (1995): 2699-2703.

[28] Arbizzani, Catia, M. Mastragostino, and F. Soavi. "New trends in electrochemical supercapacitors." Journal of power sources 100.1 (2001): 164-170.

[29] Arbizzani, Catia, Marina Mastragostino, and Luca Meneghello. "Polymer-based redox supercapacitors: A comparative study." Electrochimica Acta41.1 (1996): 21-26.

[30] Palacios, Tomás, Allen Hsu, and Han Wang. "Applications of graphene devices in RF communications." Communications Magazine, IEEE 48.6 (2010): 122-128.

[31] Jayalakshmi, M., and K. Balasubramanian. "Simple capacitors to supercapacitors-an overview." Int. J. Electrochem. Sci 3.11 (2008): 1196-1217.

[32] Raistrick, Ian D., and Ruth J. Sherman. "Electrical response of electrochemical capacitors based on high surface area ruthenium oxide electrodes." Proceedings of the 1987 Electrochemical Society spring meeting: Extended abstracts. Volume 87-1. 1987.

[33] McHardy, John, and Frank Ludwig. "Electrochemistry of semiconductors and electronics." Noyes, Park Ridge, NJ (1992).

[34] Tong, R. R., et al. "Power source characteristics of the ultracapacitor." 33rd International Power Sources Symposium. Vol. 1. 1988.

[35] Goodwin, M. L., and R. L. Keenan. "Development of PRI Ultracapacitors for SLI and Other Automotive Applications." Proceedings of the Fourth International Seminar on Double Layer Capacitors and Similar Energy Storage Devices, Deerfield Beach, Florida.1994.

[36] Trasatti, Sergio, and Giovanni Buzzanca. "Ruthenium dioxide: a new interesting electrode material. Solid state structure and electrochemical behaviour." Journal of Electroanalytical Chemistry and Interfacial Electrochemistry 29.2 (1971): A1-A5.

[37] Gujar, T. P., et al. "Electrochemically deposited nanograin ruthenium oxide as a pseudocapacitive electrode." International Journal of Electrochemical Science 2.9 (2007): 666-673.

[38] Zheng, J. P., and T. R. Jow. "A new charge storage mechanism for electrochemical capacitors." Journal of the Electrochemical Society 142.1 (1995): L6-L8.

[39] Bi, Rong-Rong, et al. "Highly dispersed RuO_2 nanoparticles on carbon nanotubes: facile synthesis and enhanced supercapacitance performance."The Journal of Physical Chemistry C 114.6 (2010): 2448-2451.

[40] Mayrand-Provencher, Laurence, and Dominic Rochefort. "Influence of the conductivity and viscosity of protic ionic liquids electrolytes on the pseudocapacitance of RuO_2 electrodes." The Journal of Physical Chemistry C 113.4 (2009): 1632-1639.

[41] Hu, Chi-Chang, et al. "Design and tailoring of the nanotubular arrayed architecture of hydrous RuO_2 for next generation supercapacitors." Nano letters 6.12 (2006): 2690-2695.

[42] Chen, Pochiang, et al. "Inkjet printing of single-walled carbon nanotube/RuO_2 nanowire supercapacitors on cloth fabrics and flexible substrates." Nano Research 3.8 (2010): 594-603.

[43] Liu, Yang, Weiwei Zhao, and Xiaogang Zhang. "Soft template synthesis of mesoporous Co_3O_4/$RuO_2.xH_2O$ composites for electrochemical capacitors." Electrochimica Acta 53.8 (2008): 3296-3304.

[44] Zhang, Xiaojun, et al. "Synthesis of porous NiO nanocrystals with controllable surface area and their application as supercapacitor electrodes."Nano Research 3.9 (2010): 643-652.

[45] Nam, Kyung-Wan, and Kwang-Bum Kim. "A study of the preparation of NiO_x electrode via electrochemical route for supercapacitor applications and their charge storage mechanism." Journal of the Electrochemical Society149.3 (2002): A346-A354.

[46] Pang, Suh-Cem, Marc A. Anderson, and Thomas W. Chapman. "Novel electrode materials for thin-film ultracapacitors: comparison of electrochemical properties of sol-gel-derived and electrodeposited manganese dioxide." Journal of the Electrochemical Society 147.2 (2000): 444-450.

[47] Chen, Po-Chiang, et al. "Preparation and characterization of flexible asymmetric supercapacitors based on transition-metal-oxide nanowire/single-walled carbon nanotube hybrid thin-film electrodes." ACS nano 4.8 (2010): 4403-4411.

[48] Du, Xuan, et al. "Electrochemical performances of nanoparticle Fe_3O_4/activated carbon supercapacitor using KOH electrolyte solution." The Journal of Physical Chemistry C 113.6 (2009): 2643-2646.

[49] Yuan, Changzhou, et al. "Ultrathin mesoporous $NiCo_2O_4$ nanosheets supported on Ni foam as advanced electrodes for supercapacitors."Advanced Functional Materials 22.21 (2012): 4592-4597.

[50] Cheng, Jinbing, et al. "Mesoporous $ZnCo_2O_4$ nanoflakes grown on nickel foam as electrodes for high performance supercapacitors." Physical Chemistry Chemical Physics 17.26 (2015): 17016-17022.

[51] Mondal, Anjon Kumar, et al. "Mesoporous $MnCo_2O_4$ with a Flake-Like Structure as Advanced Electrode Materials for Lithium-Ion Batteries and Supercapacitors." Chemistry–A European Journal 21.4 (2015): 1526-1532.

[52] Wang, Zhuo, et al. "One-step accurate synthesis of shell controllable $CoFe_2O_4$ hollow microspheres as high-performance electrode materials in supercapacitor." Nano Research: 1-8.

[53] Xu, Z. P., and H. C. Zeng. "Control of surface area and porosity of Co_3O_4 via intercalation of oxidative or nonoxidative anions in hydrotalcite-like precursors." Chemistry of materials 12.11 (2000): 3459-3465.

[54] Wöllenstein, J., et al. "Cobalt oxide based gas sensors on silicon substrate for operation at low temperatures." Sensors and Actuators B: Chemical 93.1 (2003): 442-448.

[55] Chen, Jia, Xifan Wu, and Annabella Selloni. "Electronic structure and bonding properties of cobalt oxide in the spinel structure." Physical Review B83.24 (2011): 245204.

[56] Roth, W. L. "The magnetic structure of Co_3O_4." Journal of Physics and Chemistry of Solids 25.1 (1964): 1-10.

[57] Satio, Shinichiro, et al. "Gas sensing characteristics of porous ZnO and Pt/ZnO ceramics." Journal of the American Ceramic Society 68.1 (1985): 40-43.

[58] Shinde, V. R., et al. "Supercapacitive cobalt oxide (Co_3O_4) thin films by spray pyrolysis." Applied Surface Science 252.20 (2006): 7487-7492.

[59] Kwang Joo Kim and Young Ran Park, Solid State Communications 127, 25-28 (2003).

[60] Cheng, Hua, et al. "A facile method to improve the high rate capability of Co_3O_4 nanowire array electrodes." Nano Research 3.12 (2010): 895-901.

[61] Wei, Te-Yu, et al. "Cobalt oxide aerogels of ideal supercapacitive properties prepared with an epoxide synthetic route." Chemistry of Materials 21.14 (2009): 3228-3233.

[62] Xu, Juan, et al. "Preparation and electrochemical capacitance of cobalt oxide (Co_3O_4) nanotubes as supercapacitor material." Electrochimica Acta56.2 (2010): 732-736.

[63] Gao, Yinyi, et al. "Electrochemical capacitance of Co_3O_4 nanowire arrays supported on nickel foam." Journal of Power Sources 195.6 (2010): 1757-1760.

[64] Wang, Guoxiu, et al. "Hydrothermal synthesis and optical, magnetic, and supercapacitance properties of nanoporous cobalt oxide nanorods." The Journal of Physical Chemistry C 113.11 (2009): 4357-4361.

[65] Cui, Li, Juan Li, and Xiao-Gang Zhang. "Preparation and properties of Co_3O_4 nanorods as supercapacitor material." Journal of applied electrochemistry39.10 (2009): 1871-1876.

[66] Shinde, V. R., et al. "Supercapacitive cobalt oxide (Co_3O_4) thin films by spray pyrolysis." Applied Surface Science 252.20 (2006): 7487-7492.

[67] Wei, Te-Yu, et al. "Cobalt oxide aerogels of ideal supercapacitive properties prepared with an epoxide synthetic route." Chemistry of Materials 21.14 (2009): 3228-3233.

[68] Zheng, Ming-bo, et al. "Preparation of mesoporous Co_3O_4 nanoparticles via solid− liquid route and effects of calcination temperature and textural parameters on their electrochemical capacitive behaviors." The Journal of Physical Chemistry C 113.9 (2009): 3887-3894.

[69] Xiong, Shenglin, et al. "Controllable synthesis of mesoporous Co_3O_4 nanostructures with tunable morphology for application in supercapacitors."Chemistry–A European Journal 15.21 (2009): 5320-5326.

[70] Tavares, A. C., et al. "Electrochemical study of spinel oxide systems with nominal compositions $Ni_{1-x}Cu_xCo_2O_4$ and $NiCo_{2-y}Cu_yO_4$." Journal of Solid State Electrochemistry 5.1 (2001): 57-67.

[71] Xia, Xin-hui, et al. "Self-supported hydrothermal synthesized hollow Co_3O_4 nanowire arrays with high supercapacitor capacitance." Journal of Materials Chemistry 21.25 (2011): 9319-9325.

[72] Hamdani, M., et al. "Physicochemical and electrocatalytic properties of Li-Co_3O_4 anodes prepared by chemical spray pyrolysis for application in alkaline water electrolysis." Electrochimica acta 49.9 (2004): 1555-1563.

[73] Lapham, D. P., et al. "The preparation of $NiCo_2O_4$ films by electrostatic spray deposition." Thin Solid Films 391.1 (2001): 17-20.

[74] Singh, N. K., J. P. Singh, and R. N. Singh. "Sol–gel-derived spinel Co_3O_4 films and oxygen evolution: Part II. Optimization of preparation conditions and influence of the nature of the metal salt precursor." International journal of hydrogen energy 27.9 (2002): 895-903.

[75] Chi, Bo, et al. "Effect of precipitant on preparation of Ni–Co spinel oxide by coprecipitation method." Materials Letters 58.9 (2004): 1415-1418.

[76] Guan, Hongyu, et al. "Fabrication of $NiCo_2O_4$ nanofibers by electrospinning." Solid-state communications 131.2 (2004): 107-109.

[77] Kibria, AKM Fazle, and S. A. Tarafdar. "Electrochemical studies of a nickel–copper electrode for the oxygen evolution reaction (OER)." International journal of hydrogen energy 27.9 (2002): 879-884.

[78] Yuan, Zhengyong, et al. "Synthesis and electrochemical performance of nanosized Co_3O_4." Materials Chemistry and Physics 79.1 (2003): 1-4.

[79] Jiang, Yang, et al. "Moderate temperature synthesis of nanocrystalline Co_3O_4 via gel hydrothermal oxidation." Materials chemistry and physics 74.2 (2002): 234-237.

[80] Castro, E. B., S. G. Real, and LF Pinheiro Dick. "Electrochemical characterization of porous nickel–cobalt oxide electrodes." International journal of hydrogen energy 29.3 (2004): 255-261.

[81] Mondal, Anjon Kumar. Electrode Materials for Lithium-ion Batteries and Supercapacitors. Diss. University of Technology, Sydney, 2015.

[82] Hu, Michael Z-C., Michael T. Harris, and Charles H. Byers. "Nucleation and growth for synthesis of nanometric zirconia particles by forced hydrolysis."Journal of colloid and interface science 198.1 (1998): 87-99.

[83] Roy, Mouni, Sourav Ghosh, and Milan Kanti Naskar. "Synthesis of morphology controllable porous Co_3O_4 nanostructures with tunable textural properties and their catalytic application." Dalton Transactions 43.26 (2014): 10248-10257.

[84] Sun, Jingxue, et al. "Bismuth vanadate hollow spheres: Bubble template synthesis and enhanced photocatalytic properties for photodegradation."Applied Catalysis B: Environmental 132 (2013): 304-314.

[85] Zhou, Chao, et al. "Bubble template synthesis of $Sn_2Nb_2O_7$ hollow spheres for enhanced visible-light-driven photocatalytic hydrogen production." Chemical Communications 49.84 (2013): 9872-9874.

[86] Kakiuchi, Keita, et al. "Fabrication of mesoporous ZnO nanosheets from precursor templates grown in aqueous solutions." Journal of Sol-Gel Science and Technology 39.1 (2006): 63-72.

[87] Marinho, J. Z., et al. "Urea-based synthesis of zinc oxide nanostructures at low temperature." Journal of Nanomaterials 2012 (2012): 3.

[88] Kolen'ko, Yu V., et al. "Photocatalytic properties of titania powders prepared by hydrothermal method." Applied Catalysis B: Environmental 54.1 (2004): 51-58.

[89] Culebras, Mario, Clara M. Gómez, and Andrés Cantarero. "Review on polymers for thermoelectric applications." Materials 7.9 (2014): 6701-6732.

[90] Miki, Yasuhiro, et al. "Amorphous MoS_2 as the cathode of lithium secondary batteries." Journal of power sources 54.2 (1995): 508-510.

[91] Dubal, Deepak P., et al. "Nickel cobaltite as an emerging material for supercapacitors: An overview." Nano Energy 11 (2015): 377-399.

[92] Hadke, Shreyash, et al. "Role of fuel and fuel-to-oxidizer ratio in combustion synthesis of nano-crystalline nickel oxide powders." Ceramics International41.10 (2015): 14949-14957.

[93] Štěpánek, František, Miloš Marek, and Pierre M. Adler. "Modeling capillary condensation hysteresis cycles in reconstructed porous media." AIChE journal 45.9 (1999): 1901-1912.

[94] Gubbins, Keith E. "Hysteresis Phenomena in Mesoporous Materials." (2009).

[95] Grosman, Annie, and Camille Ortega. "Capillary condensation in porous materials. Hysteresis and interaction mechanism without pore blocking/percolation process." Langmuir 24.8 (2008): 3977-3986.

[96] Kleitz, Freddy, et al. "Probing adsorption, pore condensation, and hysteresis behavior of pure fluids in three-dimensional cubic mesoporous KIT-6 silica."The Journal of Physical Chemistry C 114.20 (2010): 9344-9355.

[97] Wang, Guoxiu, et al. "Graphene nanosheets for enhanced lithium storage in lithium ion batteries." Carbon 47.8 (2009): 2049-2053.

[98] Hadjiev, V. G., M. N. Iliev, and I. V. Vergilov. "The Raman spectra of Co_3O_4." Journal of Physics C: Solid State Physics 21.7 (1988): L199.

[99] Ramana, C. V., M. Massot, and C. M. Julien. "XPS and Raman spectroscopic characterization of $LiMn_2O_4$ spinels." Surface and interface analysis 37.4 (2005): 412-416.

[100] Stanojević, ZV Marinković, N. Romčević, and B. Stojanović. "Spectroscopic study of spinel ZnCr 2 O 4 obtained from mechanically activated ZnO–Cr_2O_3 mixtures." Journal of the European Ceramic Society 27.2 (2007): 903-907.

[101] Wang, Guoxiu, et al. "Hydrothermal synthesis and optical, magnetic, and supercapacitance properties of nanoporous cobalt oxide nanorods." The Journal of Physical Chemistry C 113.11 (2009): 4357-4361.

[102] Lin, Hung-Kuan, et al. "Synthesis, characterization and catalytic oxidation of carbon monoxide over cobalt oxide." Catalysis letters 88.3-4 (2003): 169-174.

[103] Spencer, Charles D., and Dietrich Schroeer. "Mössbauer study of several cobalt spinels using Co 57 and Fe 57." Physical Review B 9.9 (1974): 3658.

[104] Kurtulus, F., and H. Guler. "A simple microwave-assisted route to prepare black cobalt, Co_3O_4." Inorganic materials 41.5 (2005): 483-485.

[105] St G, Christoskova, et al. "Preparation and characterization of a higher cobalt oxide." Materials chemistry and physics 60.1 (1999): 39-43.

[106] Xiao, Junwu, and Shihe Yang. "Sequential crystallization of sea urchin-like bimetallic (Ni, Co) carbonate hydroxide and its morphology conserved conversion to porous $NiCo_2O_4$ spinel for pseudocapacitors." RSC Advances 1.4 (2011): 588-595.

[107] Liu, Xiangmei, et al. "Facile and green synthesis of mesoporous Co_3O_4 nanocubes and their applications for supercapacitors." Nanoscale 5.14 (2013): 6525-6529.

[108] Hu, Chi-Chang, Jia-Cing Chen, and Kuo-Hsin Chang. "Cathodic deposition of Ni $(OH)_2$ and $Co(OH)_2$ for asymmetric supercapacitors: importance of the electrochemical reversibility of redox couples." Journal of Power Sources221 (2013): 128-133.

[109] Meher, Sumanta Kumar, P. Justin, and G. Ranga Rao. "Nanoscale morphology dependent pseudocapacitance of NiO: Influence of intercalating anions during synthesis." Nanoscale 3.2 (2011): 683-692.

[110] Randles, J. E_B_. "A cathode ray polarograph. Part II. —The current-voltage curves." Transactions of the Faraday Society 44 (1948): 327-338.

[111] Sevčik, A. "Collection Czech." Chem. Commun 13 (1948): 349.

[112] Aghazadeh, Mustafa. "Electrochemical preparation and properties of nanostructured Co_3O_4 as supercapacitor material." Journal of Applied Electrochemistry 42.2 (2012): 89-94.

[113] Tummala, Raghavender, Ramesh K. Guduru, and Pravansu S. Mohanty. "Nanostructured Co_3O_4 electrodes for supercapacitor applications from plasma spray technique." Journal of Power Sources 209 (2012): 44-51.

[114] Gomez, Jamie, and Egwu E. Kalu. "High-performance binder-free Co–Mn composite oxide supercapacitor electrode." Journal of Power Sources 230 (2013): 218-224.

[115] Candy, J-P., et al. "The pore texture of Raney-nickel determined by impedance measurements." Electrochimica Acta 27.11 (1982): 1585-1593.

[116] Deng, Jiachun, et al. "Solution combustion synthesis of cobalt oxides (Co_3O_4 and Co_3O_4/CoO) nanoparticles as supercapacitor electrode materials." Electrochimica Acta 132 (2014): 127-135.

[117] Wu, J. B., et al. "Pseudocapacitive properties of electrodeposited porous nanowall Co_3O_4 film." Electrochimica Acta 56.20 (2011): 7163-7170.

[118] Xia, Xin-hui, et al. "Self-supported hydrothermal synthesized hollow Co_3O_4nanowire arrays with high supercapacitor capacitance." Journal of Materials Chemistry 21.25 (2011): 9319-9325.

[119] Pang, Huan, et al. "Dendrite-like Co_3O_4 nanostructure and its applications in sensors, supercapacitors and catalysis." Dalton Transactions 41.19 (2012): 5862-5868.

[120] Liu, Xiangmei, et al. "Facile and green synthesis of mesoporous Co_3O_4 nanocubes and their applications for supercapacitors." Nanoscale 5.14 (2013): 6525-6529.

[121] Du, Wei, et al. "Facile synthesis of hollow Co_3O_4 boxes for high capacity supercapacitor." Journal of Power Sources 227 (2013): 101-105.

[122] Balasubramanian, Sethuraman, and Purushothaman Kamatchi Kamaraj. "Fabrication of natural polymer assisted mesoporous Co_3O_4/carbon composites for supercapacitors." Electrochimica Acta 168 (2015): 50-58.

[123] Ma, Lianbo, et al. "Facile synthesis of Co_3O_4 porous nanosheets/reduced graphene oxide composites and their excellent supercapacitor performance."RSC Advances 4.95 (2014): 53180-53187.

[124] Liu, Jinping, et al. " Co_3O_4 Nanowire@ MnO_2 Ultrathin Nanosheet Core/Shell Arrays: A New Class of High-Performance Pseudocapacitive Materials."Advanced Materials 23.18 (2011): 2076-2081.

[125] Gupta, Ram K., et al. "Flexible and High Performance Supercapacitors Based on $NiCo_2O_4$for Wide Temperature Range Applications." Scientific reports 5 (2015).